



**HAL**  
open science

## Long-term thermal sensitivity of Earth's tropical forests

Martin J P Sullivan, Simon Lewis, Kofi Affum-Baffoe, Carolina Castilho, Flávia Costa, Aida Cuni Sanchez, Corneille Ewango, Wannex Hubau, Beatriz Marimon, Abel Monteagudo-Mendoza, et al.

► **To cite this version:**

Martin J P Sullivan, Simon Lewis, Kofi Affum-Baffoe, Carolina Castilho, Flávia Costa, et al.. Long-term thermal sensitivity of Earth's tropical forests. *Science*, 2020, 368 (6493), pp.869-874. 10.1126/science.aaw7578 . hal-02650649

**HAL Id: hal-02650649**

**<https://hal.umontpellier.fr/hal-02650649v1>**

Submitted on 16 Aug 2024

**HAL** is a multi-disciplinary open access archive for the deposit and dissemination of scientific research documents, whether they are published or not. The documents may come from teaching and research institutions in France or abroad, or from public or private research centers.

L'archive ouverte pluridisciplinaire **HAL**, est destinée au dépôt et à la diffusion de documents scientifiques de niveau recherche, publiés ou non, émanant des établissements d'enseignement et de recherche français ou étrangers, des laboratoires publics ou privés.

## Long-term thermal sensitivity of Earth's tropical forests

Martin J. P. Sullivan<sup>1,2</sup>, Simon L. Lewis<sup>1,3</sup>, Kofi Affum-Baffoe<sup>4</sup>, Carolina Castilho<sup>5</sup>, Flávia Costa<sup>6</sup>, Aida Cuni Sanchez<sup>7,8</sup>, Corneille E. N. Ewango<sup>9,10,11</sup>, Wannes Hubau<sup>1,12,13</sup>, Beatriz Marimon<sup>14</sup>, Abel Monteagudo-Mendoza<sup>15</sup>, Lan Qie<sup>16</sup>, Bonaventure Sonké<sup>17</sup>, Rodolfo Vasquez Martinez<sup>15</sup>, Timothy R Baker<sup>1</sup>, Roel J. W. Brienen<sup>1</sup>, Ted R. Feldpausch<sup>18</sup>, David Galbraith<sup>1</sup>, Manuel Gloor<sup>1</sup>, Yadvinder Malhi<sup>19</sup>, Shin-Ichiro Aiba<sup>20</sup>, Miguel N. Alexiades<sup>21</sup>, Everton C. Almeida<sup>22</sup>, Edmar Almeida de Oliveira<sup>23</sup>, Esteban Álvarez Dávila<sup>24</sup>, Patricia Alvarez Loayza<sup>25</sup>, Ana Andrade<sup>26</sup>, Simone Aparecida Vieira<sup>27</sup>, Luiz Aragão<sup>28</sup>, Alejandro Araujo-Murakami<sup>29</sup>, Eric J.M.M. Arets<sup>30</sup>, Luzmila Arroyo<sup>31</sup>, Peter Ashton<sup>32</sup>, Gerardo Aymard C.<sup>33</sup>, Fabrício B. Baccaro<sup>34</sup>, Lindsay F. Banin<sup>35</sup>, Christopher Baraloto<sup>36</sup>, Plínio Barbosa Camargo<sup>37</sup>, Jos Barlow<sup>38</sup>, Jorcely Barroso<sup>39</sup>, Jean-François Bastin<sup>40</sup>, Sarah A. Batterman<sup>1,41,42,43</sup>, Hans Beeckman<sup>12</sup>, Serge K. Begne<sup>17,44</sup>, Amy C. Bennett<sup>44</sup>, Erika Berenguer<sup>19,38</sup>, Nicholas Berry<sup>45</sup>, Lilian Blanc<sup>46</sup>, Pascal Boeckx<sup>47</sup>, Jan Bogaert<sup>48</sup>, Damien Bonal<sup>49</sup>, Frans Bongers<sup>50</sup>, Matt Bradford<sup>51</sup>, Francis Q. Brearley<sup>2</sup>, Terry Brncic<sup>52</sup>, Foster Brown<sup>53</sup>, Benoit Burban<sup>54</sup>, José Luís Camargo<sup>26</sup>, Wendeson Castro<sup>55</sup>, Carlos Céron<sup>56</sup>, Sabina Cerruto Ribeiro<sup>57</sup>, Victor Chama Moscoso<sup>15</sup>, Jérôme Chave<sup>58</sup>, Eric Chezeaux<sup>59</sup>, Connie J. Clark<sup>25</sup>, Fernanda Coelho<sup>1</sup>, Murray Collins<sup>61</sup>, James A. Comiskey<sup>62,63</sup>, Fernando Cornejo Valverde<sup>64</sup>, Massiel Corrales Medina<sup>65</sup>, Lola da Costa<sup>66</sup>, Martin Dančák<sup>67</sup>, Greta C. Dargie<sup>1</sup>, Stuart Davies<sup>68</sup>, Nallaret Davila Cardozo<sup>69</sup>, Thales de Haulleville<sup>12,48</sup>, Marcelo Brilhante de Medeiros<sup>70</sup>, Jhon del Aguila Pasquel<sup>71</sup>, Géraldine Derroire<sup>72</sup>, Anthony Di Fiore<sup>73</sup>, Jean-Louis Doucet<sup>74</sup>, Aurélie Dourdain<sup>72</sup>, Vincent Droissant<sup>75</sup>, Luisa Fernanda Duque<sup>76</sup>, Romeo Ekoungoulou<sup>77</sup>, Fernando Elias<sup>78</sup>, Terry Erwin<sup>79</sup>, Adriane Esquivel-Muelbert<sup>80</sup>, Sophie Fauset<sup>81</sup>, Joice Ferreira<sup>82</sup>, Gerardo Flores Llampazo<sup>83</sup>, Ernest Folli<sup>84</sup>, Andrew Ford<sup>51</sup>, Martin Gilpin<sup>1</sup>, Jefferson S. Hall<sup>85</sup>, Keith C. Hamer<sup>86</sup>, Alan C. Hamilton<sup>87</sup>, David J. Harris<sup>88</sup>, Terese B. Hart<sup>89,90</sup>, Radim Hédli<sup>91,92</sup>, Bruno Herault<sup>72</sup>, Rafael Herrera<sup>93</sup>, Niro Higuchi<sup>6</sup>, Annette Hladik<sup>94</sup>, Eurídice Honorio Coronado<sup>71</sup>, Isau Huamantupa-Chuquimaco<sup>95</sup>, Walter Huaraca Huasco<sup>95</sup>, Kathryn J. Jeffery<sup>96</sup>, Eliana Jimenez-Rojas<sup>97</sup>, Michelle Kalamandeen<sup>1</sup>, Marie-Noel Kamdem<sup>11,13,17,98</sup>, Elizabeth Kearsley<sup>99</sup>, Ricardo Keichi Umetsu<sup>100</sup>, Lip Khoon Kho Khoo<sup>101</sup>, Timothy Killeen<sup>102</sup>, Kanehiro Kitayama<sup>103</sup>, Bente Klitgaard<sup>104</sup>, Nicolas Labrière<sup>58</sup>, William Laurance<sup>105</sup>, Susan Laurance<sup>105</sup>, Miguel E. Leal<sup>106</sup>, Aurora Levesley<sup>1</sup>, Adriano J. N. Lima<sup>6</sup>, Janvier Lisingo<sup>11</sup>, Aline P. Lopes<sup>107,108</sup>, Gabriela Lopez-Gonzalez<sup>1</sup>, Tom Lovejoy<sup>109</sup>, Jon Lovett<sup>1</sup>, Richard Lowe<sup>110</sup>, William E. Magnusson<sup>111</sup>, Jagoba Malumbres-Olarte<sup>112,113</sup>, Ângelo Gilberto Manzatto<sup>114</sup>, Ben Hur Marimon Junior<sup>115</sup>, Andrew R. Marshall<sup>8,116,117</sup>, Toby Marthews<sup>118</sup>, Simone Matias de Almeida Reis<sup>14,19</sup>, Colin Maycock<sup>119</sup>, Karina Melgaço<sup>1</sup>, Casimiro Mendoza<sup>120</sup>, Faizah Metali<sup>121</sup>, Vianet Mihindou<sup>122,123</sup>, William Milliken<sup>104</sup>, Edward Mitchard<sup>124</sup>, Paulo S. Morandi<sup>14</sup>, Hannah L. Mossman<sup>2</sup>, Laszlo Nagy<sup>125</sup>, Henrique Nascimento<sup>6</sup>, David Neill<sup>126</sup>, Reuben Nilus<sup>127</sup>, Percy Núñez Vargas<sup>95</sup>, Walter Palacios<sup>128</sup>, Nadir Pallqui Camacho<sup>1,95</sup>, Julie Peacock<sup>1</sup>, Colin Pendry<sup>129</sup>, Maria Cristina Peñuela Mora<sup>130</sup>, Georgia C. Pickavance<sup>1</sup>, John Pipoly<sup>131</sup>, Nigel Pitman<sup>132</sup>, Maureen Playfair<sup>133</sup>, Lourens Poorter<sup>134</sup>, John R. Poulsen<sup>25</sup>, Axel D. Poulsen<sup>135</sup>, Richard Preziosi<sup>2</sup>, Adriana Prieto<sup>136</sup>, Richard Primack<sup>137</sup>, Hirma Ramírez-Angulo<sup>138</sup>, Jan Reitsma<sup>139</sup>, Maxime Réjou-Méchain<sup>75</sup>, Zorayda Restrepo Correa<sup>140</sup>, Thaiane Rodrigues de Sousa<sup>6</sup>, Lily Rodriguez Bayona<sup>141</sup>, Anand Roopsind<sup>142</sup>, Agustín Rudas<sup>136</sup>, Ervan Rutishauser<sup>42,143</sup>, Kamariah Abu Salim<sup>121</sup>, Rafael P. Salomão<sup>144,145</sup>, Juliana Schiatti<sup>6</sup>, Douglas Sheil<sup>146</sup>, Richarlly C. Silva<sup>57,147</sup>, Javier Silva Espejo<sup>148</sup>, Camila Silva Valeria<sup>38</sup>, Marcos Silveira<sup>57</sup>, Murielle Simo-Droissart<sup>17</sup>, Marcelo Fragomeni Simon<sup>70</sup>, James Singh<sup>149</sup>, Yahn Carlos Soto Shareva<sup>15</sup>, Clement Stahl<sup>54</sup>, Juliana Stropp<sup>150</sup>, Rahayu Sukri<sup>121</sup>, Terry Sunderland<sup>151,152</sup>, Martin Svátek<sup>153</sup>, Michael D. Swaine<sup>154</sup>, Varun Swamy<sup>155</sup>, Hermann Taedoum<sup>17</sup>, Joey Talbot<sup>1</sup>, James Taplin<sup>156</sup>, David Taylor<sup>157</sup>, Hans ter Steege<sup>158,159</sup>, John Terborgh<sup>25</sup>, Raquel Thomas<sup>142</sup>, Sean C. Thomas<sup>160</sup>, Armando Torres-Lezama<sup>161</sup>, Peter Umunay<sup>162,163</sup>, Luis Valenzuela Gamarra<sup>15</sup>, Geertje van der Heijden<sup>164</sup>, Peter van der Hout<sup>165</sup>, Peter van der Meer<sup>166</sup>, Mark van Nieuwstadt<sup>167</sup>, Hans Verbeeck<sup>99</sup>, Ronald Vernimmen<sup>168</sup>, Alberto Vicentini<sup>6</sup>, Ima Célia Guimarães Vieira<sup>145</sup>, Emilio Vilanova Torre<sup>169</sup>, Jason Vleminckx<sup>36</sup>, Vincent Vos<sup>171</sup>, Ophelia Wang<sup>172</sup>, Lee J. T. White<sup>123,173,174</sup>, Simon Willcock<sup>175</sup>, John T. Woods<sup>176</sup>, Verginia Wortel<sup>177</sup>, Kenneth Young<sup>178</sup>, Roderick Zagt<sup>179</sup>, Lise Zemagho<sup>17</sup>, Pieter A. Zuidema<sup>50</sup>, Joeri A. Zwarts<sup>177,180</sup>, Oliver L. Phillips<sup>1</sup>

Affiliations:

- 1 School of Geography, University of Leeds, Leeds, UK
- 2 Department of Natural Sciences, Manchester Metropolitan University, Manchester, UK
- 3 Department of Geography, University College London, London, UK
- 4 Mensuration Unit, Forestry Commission of Ghana, Kumasi, Ghana
- 5 Embrapa Roraima, Brazilian Agricultural Research Corporation (EMBRAPA), Brasília, Brazil
- 6 Instituto Nacional de Pesquisas da Amazônia (INPA), Manaus, Brazil
- 7 Department of Ecosystem Science and Sustainability, Colorado State University, USA
- 8 Department of Environment and Geography, University of York, York, UK
- 9 DR Congo Programme, Wildlife Conservation Society, Kisangani, Democratic Republic of Congo
- 10 Centre de Formation et de Recherche en Conservation Forestiere (CEFRECOF), Epulu, Democratic Republic of Congo
- 11 Faculté de Gestion de Ressources Naturelles Renouvelables, Université de Kisangani, Kisangani, Democratic Republic of Congo
- 12 Service of Wood Biology, Royal Museum for Central Africa, Tervuren, Belgium
- 13 Department of Environment, Laboratory of Wood Technology (Woodlab), Ghent University, Ghent, Belgium
- 14 Faculdade de Ciências Agrárias, Biológicas e Sociais Aplicadas, Universidade do Estado de Mato Grosso, Nova Xavantina-MT, Brazil
- 15 Jardín Botánico de Missouri, Oxapampa, Peru
- 16 School of Life Sciences, University of Lincoln, Lincoln, UK
- 17 Plant Systematics and Ecology Laboratory, Higher Teachers' Training College, University of Yaoundé I, Yaoundé, Cameroon
- 18 Geography, College of Life and Environmental Sciences, University of Exeter, Exeter, UK
- 19 Environmental Change Institute, School of Geography and the Environment, University of Oxford, Oxford, UK
- 20 Graduate School of Science and Engineering, Kagoshima University, Japan
- 21 School of Anthropology and Conservation, University of Kent, Canterbury, UK
- 22 Instituto de Biodiversidade e Florestas, Universidade Federal do Oeste do Pará, Santarém - PA, Brazil
- 23 Universidade do Estado de Mato Grosso, Cáceres - MT, Brazil
- 24 Escuela de Ciencias Agrícolas, Pecuarias y del Medio Ambiente, National Open University and Distance, Colombia
- 25 Center for Tropical Conservation, Nicholas School of the Environment, Duke University, Durham, NC, USA
- 26 Projeto Dinâmica Biológica de Fragmentos Florestais, Instituto Nacional de Pesquisas da Amazônia, Manaus, Brazil
- 27 Universidade Estadual de Campinas, Campinas - SP, Brazil
- 28 National Institute for Space Research (INPE), São José dos Campos-SP, Brazil
- 29 Museo de Historia Natural Noel Kempff Mercado, Universidad Autónoma Gabriel René Moreno, Santa Cruz, Bolivia
- 30 Wageningen Environmental Research, Wageningen, The Netherlands
- 31 Dirección de la Carrera de Biología, Universidad Autónoma Gabriel René Moreno, Santa Cruz, Bolivia
- 32 Department of Organismic and Evolutionary Biology, Harvard University, Cambridge, MA, USA
- 33 Programa de Ciencias del Agro y el Mar, Herbario Universitario, Barinas, Venezuela
- 34 Departamento de Biologia, Universidade Federal do Amazonas, Manaus, Brazil

- 35 Centre of Ecology and Hydrology, Penicuik, UK
- 36 International Center for Tropical Botany, Department of Biological Sciences, Florida International University, Florida, FL, USA
- 37 Centro de Energia Nuclear na Agricultura, Universidade de São Paulo, São Paulo, SP, Brazil
- 38 Lancaster Environment Centre, Lancaster University, Lancaster, UK
- 39 Centro Multidisciplinar, Universidade Federal do Acre, Cruzeiro do Sul - AC, Brazil
- 40 Institute of Integrative Biology, ETH Zurich, Zurich, Switzerland
- 41 Priestley International Centre for Climate, University of Leeds, Leeds, UK
- 42 Smithsonian Tropical Research Institute, Panama, Panama
- 43 Cary Institute of Ecosystem Studies, Millbrook, NY, USA
- 44 School of Geography, School of Geography, Leeds, UK
- 45 The Landscapes and Livelihoods Group, Edinburgh, UK
- 46 UR Forest & Societies, CIRAD, Montpellier, France
- 47 Isotope Bioscience Laboratory-ISOFYS, Ghent University, Ghent, Belgium
- 48 Gembloux Agro-Bio Tech, University of Liège, Liège, Belgium
- 49 UMR Silva, INRA, Nancy, France
- 50 Department of Forest Ecology and Forest Management Group, Wageningen University, Wageningen, The Netherlands
- 51 CSIRO, Canberra, Australia
- 52 Congo Programme, Wildlife Conservation Society, Brazzaville, Republic of Congo
- 53 Woods Hole Research Center, Falmouth, MA, USA
- 54 Ecologie des Forêts de Guyane (ECOFOG), INRA, Kourou, French Guiana
- 55 Programa de Pós-Graduação Ecologia e Manejo de Recursos Naturais, Universidade Federal do Acre, Rio Branco - AC, Brazil
- 56 Herbario Alfredo Paredes, Universidad Central del Ecuador, Quito, Ecuador
- 57 Centro de Ciências Biológicas e da Natureza, Universidade Federal do Acre, Rio Branco - AC, Brazil
- 58 Laboratoire Évolution et Diversité Biologique - UMR 5174 (CNRS/IRD/UPS), CNRS, Toulouse, France
- 59 Rougier-Gabon, Libreville, Gabon
- 60 Nicholas School of the Environment, Duke University, Durham, NC, USA
- 61 Grantham Research Institute on Climate Change and the Environment, London, UK
- 62 Inventory & Monitoring Program, National Park Service, Fredericksburg, VA, USA
- 63 Smithsonian Institution, Washington, DC, USA
- 64 Proyecto Castaña, Madre de Dios, Peru
- 65 Universidad Nacional de San Agustín de Arequipa, Arequipa, Peru
- 66 Instituto de Geociências, Faculdade de Meteorologia, Universidade Federal do Pará, Belém - PA, Brazil
- 67 Faculty of Science, Department of Ecology and Environmental Sciences, Palacký University Olomouc, Olomouc, Czech Republic
- 68 Center for Tropical Forest Science, Smithsonian Tropical Research Institute, Panama, Panama
- 69 Facultad de Ciencias Biológicas, Universidad Nacional de la Amazonía Peruana, Iquitos, Peru
- 70 Embrapa Genetic Resources & Biotechnology, Brazilian Agricultural Research Corporation (EMBRAPA), Brasília, Brazil
- 71 Instituto de Investigaciones de la Amazonía Peruana, Iquitos, Peru
- 72 Ecologie des Forêts de Guyane (ECOFOG), CIRAD, Kourou, French Guiana

- 73 Department of Anthropology, The University of Texas at Austin, Austin, TX, USA
- 74 Forest Resources Management, Gembloux Agro-Bio Tech, University of Liège, Liège, Belgium
- 75 AMAP Lab, IRD, CIRAD, CNRS, INRA, Univ Montpellier, Montpellier, France
- 76 Socioecosistemas y Cambio Climatico, Fundacion con Vida, Medellín, Colombia
- 77 School of Forestry, Beijing Forestry University, Beijing, China
- 78 Institute of Biological Sciences, Universidade Federal do Pará, Belém - PA, Brazil
- 79 National Museum of Natural History, Smithsonian Institute, Washington, DC, USA
- 80 School of Geography, Earth and Environmental Sciences, University of Birmingham, Birmingham, UK
- 81 School of Geography, Earth and Environmental Sciences, University of Plymouth, Plymouth, UK
- 82 Embrapa Amazônia Oriental, Brazilian Agricultural Research Corporation (EMBRAPA), Brasília, Brazil
- 83 Universidad Nacional Jorge Basadre de Grohmann (UNJBG), Tacna, Peru
- 84 Forestry Research Institute of Ghana (FORIG), Kumasi, Ghana
- 85 Smithsonian Institution Forest Global Earth Observatory (ForestGEO), Smithsonian Tropical Research Institute, Washington, DC, USA
- 86 School of Biology, University of Leeds, Leeds, UK
- 87 128 Busbridge Lane, Godalming, Surrey, UK
- 88 Royal Botanic Garden Edinburgh, Edinburgh, UK
- 89 Lukuru Wildlife Research Foundation, Kinshasa, Democratic Republic of Congo
- 90 Division of Vertebrate Zoology, Yale Peabody Museum of Natural History, New Haven, CT, USA
- 91 Institute of Botany, Czech Academy of Sciences, Brno, Czech Republic
- 92 Department of Botany, Palacký University in Olomouc, Olomouc, Czech Republic
- 93 Instituto Venezolano de Investigaciones Científicas (IVIC), Caracas, Venezuela
- 94 Département Hommes, natures, sociétés, Muséum National d'Histoire Naturel, Paris, France
- 95 Universidad Nacional de San Antonio Abad del Cusco, Cusco, Peru
- 96 Biological and Environmental Sciences, University of Stirling, Stirling, UK
- 97 Instituto IMANI, Universidad Nacional de Colombia, Leticia, Colombia
- 98 Faculty of Science, Department of Botany and Plant Physiology, University of Buea, Buea, Cameroon
- 99 Department of Environment, Computational & Applied Vegetation Ecology (Cavelab), Ghent University, Ghent, Belgium
- 100 PELD, Universidade do Estado de Mato Grosso, Nova Xavantina-MT, Brazil
- 101 Tropical Peat Research Institute, Malaysian Palm Oil Board, Kuala Lumpur, Malaysia
- 102 Agteca, Santa Cruz, Bolivia
- 103 Graduate School of Agriculture, Kyoto University, Japan
- 104 Royal Botanic Gardens Kew, Richmond, London, UK
- 105 Centre for Tropical Environmental and Sustainability Science (TESS) and College of Marine and Environmental Sciences, James Cook University, Australia
- 106 Uganda Programme, Wildlife Conservation Society, Kampala, Uganda
- 107 Remote Sensing Division, National Institute for Space Research (INPE), São José dos Campos-SP, Brazil
- 108 Department of Ecology, University of Brasília, Brasília, Brazil
- 109 Environmental Science and Policy, George Mason University, Fairfax, VA, USA
- 110 Botany Department, University of Ibadan, Ibadan, Nigeria

- 111 Coordenação da Biodiversidade, Instituto Nacional de Pesquisas da Amazônia (INPA), Manaus,  
Brazil
- 112 cE3c – Centre for Ecology, Evolution and Environmental Changes / Azorean Biodiversity Group,  
Universidade dos Açores, Angra do Heroísmo, Azores, Portugal
- 113 LIBRe – Laboratory for Integrative Biodiversity Research, Finnish Museum of Natural History,  
University of Helsinki, Helsinki, Finland
- 114 Laboratório de Biogeoquímica Ambiental Wolfgang C. Pfeiffer, Universidade Federal de Rondônia,  
Porto Velho - RO, Brazil
- 115 Faculdade de Ciências Agrárias, Biológicas e Sociais Aplicadas, Universidad do Estado de Mato  
Grosso, Nova Xavantina-MT, Brazil
- 116 Tropical Forests and People Research Centre, University of the Sunshine Coast, Australia
- 117 Flamingo Land Ltd., North Yorkshire, UK
- 118 Centre for Ecology and Hydrology, Wallingford, UK
- 119 School of International Tropical Forestry, Universiti Malaysia Sabah, Kota Kinabalu, Malaysia
- 120 Escuela de Ciencias Forestales, Unidad Académica del Trópico, Universidad Mayor de San Simón,  
Sacta, Bolivia
- 121 Faculty of Science, Universiti Brunei Darussalam, Brunei
- 122 Agence Nationale des Parcs Nationaux, Libreville, Gabon
- 123 Ministère de la Forêt, de la Mer, de l'Environnement, Chargé du Plan Climat, Libreville, Gabon
- 124 University of Edinburgh, Edinburgh, UK
- 125 Biologia Vegetal, Universidade Estadual de Campinas, Campinas - SP, Brazil
- 126 Facultad de Ingeniería Ambiental, Universidad Estatal Amazónica, Puyo, Pastaza, Ecuador
- 127 Forest Research Centre, Sabah Forestry Department, Sepilok, Malaysia
- 128 Carrera de Ingeniería Forestal, Universidad Técnica del Norte, Ibarra, Ecuador
- 129 Royal Botanical Garden Edinburgh, Edinburgh, UK
- 130 Universidad Regional Amazónica IKIAM, Tena, Ecuador
- 131 Public Communications and Outreach Group, Parks and Recreation Division, Oakland Park, FL, USA
- 132 Keller Science Action Center, Field Museum, Chicago, IL, USA
- 133 Centre for Agricultural Research in Suriname (CELOS), Paramaribo, Suriname
- 134 Department of Forest Ecology and Forest Management Group, Wageningen University and Research,  
Wageningen, The Netherlands
- 135 University of Oslo, Oslo, Norway
- 136 Instituto de Ciencias Naturales, Universidad Nacional de Colombia, Leticia, Colombia
- 137 Department of Biology, Boston University, Boston, USA
- 138 Institute of Research for Forestry Development (INDEFOR), Universidad de los Andes, Mérida,  
Venezuela
- 139 Bureau Waardenburg, Culemborg, The Netherlands
- 140 Socioecosistemas y Cambio Climático, Fundación Con Vida, Medellín, Colombia
- 141 Centro de Conservación, Investigación y Manejo de Áreas Naturales, CIMA Cordillera Azul, Lima,  
Peru
- 142 Iwokrama International Centre for Rainforest Conservation and Development, Georgetown, Guyana
- 143 Carboforexpert, Geneva, Switzerland
- 144 Universidade Federal Rural da Amazônia/CAPEs, Belém - PA, Brazil
- 145 Museu Paraense Emílio Goeldi, Belém - PA, Brazil
- 146 Faculty of Environmental Sciences and Natural Resource Management, Norwegian University of Life  
Sciences, Ås, Norway
- 147 Instituto Federal do Acre, Rio Branco - AC, Brazil

- 148 Universidad de San Antonio Abad del Cusco, Cusco, Peru  
149 Guyana Forestry Commission, Georgetown, Guyana  
150 Federal University of Alagoas, Maceió, Brazil  
151 Sustainable Landscapes and Food Systems, Center for International Forestry Research, Bogor, Indonesia  
152 Faculty of Forestry, University of British Columbia, Vancouver, Canada  
153 Department of Forest Botany, Dendrology and Geobiocoenology, Mendel University in Brno, Brno, Czech Republic  
154 Department of Plant & Soil Science, School of Biological Sciences, University of Aberdeen, Aberdeen, UK  
155 Institute for Conservation Research, San Diego Zoo, San Diego, USA  
156 UK Research & Innovation, Innovate UK, London  
157 Department of Geography, National University of Singapore, Singapore, Singapore  
158 Naturalis Biodiversity Center, Leiden, The Netherlands  
159 Systems Ecology, VU University, Amsterdam, The Netherlands  
160 Faculty of Forestry, University of Toronto, Toronto, Canada  
161 Universidad de los Andes, Merida, Colombia  
162 Wildlife Conservation Society, New York, NY, USA  
163 Yale School of Forestry & Environmental Studies, Yale University, New Haven, CT, USA  
164 School of Geography, University of Nottingham, Nottingham, UK  
165 Van der Hout Forestry Consulting, Rotterdam, The Netherlands  
166 Van Hall Larenstein University of Applied Sciences, Velp, The Netherlands  
167 Utrecht University, Utrecht, The Netherlands  
168 Deltares, Delft, The Netherlands  
169 School of Environmental and Forest Sciences, University of Washington, Seattle, OR, USA  
170 Department of Biological Sciences, Florida International University, Florida, FL, USA  
171 Centro de Investigación y Promoción del Campesinado, La Paz, Bolivia  
172 School of Earth Sciences and Environmental Sustainability, Northern Arizona University, Flagstaff, AZ, USA  
173 Institut de Recherche en Ecologie Tropicale, Libreville, Gabon  
174 School of Natural Sciences, University of Stirling, Stirling, UK  
175 School of Natural Sciences, University of Bangor, Bangor, UK  
176 University of Liberia, Monrovia, Liberia  
177 Forest Management, Centre for Agricultural Research in Suriname (CELOS), Paramaribo, Suriname  
178 Department of Geography and The Environment, University of Texas at Austin, Austin, TX, USA  
179 Tropenbos International, Wageningen, The Netherlands  
180 Biology, Utrecht University, Utrecht, The Netherlands

1 **Abstract**

2 The sensitivity of tropical forest carbon to climate is a key uncertainty in predicting global climate  
3 change. While short-term drying and warming are known to impact forests it is unknown if such effects  
4 translate into long-term responses. Here we analyse 590 permanent plots measured across the tropics to  
5 derive the equilibrium climate controls on forest carbon. Maximum temperature is the most important  
6 predictor of aboveground biomass ( $-9.1 \text{ Mg C ha}^{-1} \text{ }^{\circ}\text{C}^{-1}$ ), primarily by reducing woody productivity, and  
7 with a greater rate of decline in the hottest forests. Our results nevertheless reveal greater thermal  
8 resilience than observations of short-term variation imply. Realising the long-term climate adaptation  
9 potential of tropical forests will require both protecting them and stabilising the Earth's climate.

10

11

12 **One sentence summary.** Biome-wide variation in tropical forest carbon stocks and dynamics shows  
13 long-term thermal resilience.



14 Main text

15 The response of tropical terrestrial carbon to environmental change is a critical component of global  
16 climate models (1). Land-atmosphere feedbacks depend on the balance of positive biomass growth  
17 stimulation by CO<sub>2</sub> fertilisation (i.e.  $\beta$ ) and negative responses to warmer temperatures and any  
18 change in precipitation (i.e.  $\gamma$ ). Yet the climate response is so poorly constrained that it remains one of  
19 the largest uncertainties in Earth system models (2, 3), with the temperature sensitivity of tropical land  
20 carbon stocks alone differing by  $> 100 \text{ Pg C } ^\circ\text{C}^{-1}$  among models (2). Such uncertainty impedes our  
21 understanding of the global carbon cycle, limiting our ability to simulate the future of the Earth  
22 system under different long-term climate mitigation strategies. A critical long-term control on tropical  
23 land-atmosphere feedbacks is the sensitivity to climate ( $\gamma$ ) of tropical forests, where c. 40 % of the  
24 world's vegetation carbon resides (4).

25 The sensitivity of tropical biomass carbon stocks, their rate of production and their persistence to  
26 environmental change can all be estimated by relating their short-term and inter-annual responses to  
27 variation in climate (5-7). These sensitivities are then used to constrain longer-term projections of  
28 climate responses (2). Such approaches typically find that higher minimum temperatures are strongly  
29 associated with slower tree growth and reduced forest carbon stocks, likely due to increased  
30 respiration at higher temperatures (7-9). Tropical forest carbon is also sensitive to precipitation (10),  
31 with, for example, elevated tree mortality occurring during drought events (11).

32 Yet, the sensitivity of ecosystems to inter-annual fluctuations may be an unreliable guide to their  
33 longer-term responses to climate change. Such responses will also be influenced by physiological  
34 acclimation (12), changes in demographic rates (13), and shifts in species composition (14). For  
35 example, both respiration and photosynthesis can acclimate under sustained temperature increases  
36 (15-17), and tropical trees exhibit physiological plasticity (18) and shifts in species composition (14)  
37 under sustained drought. These processes could mean that tropical forests are less sensitive to climate  
38 than estimates derived from inter-annual variability imply. An alternative, complimentary approach to  
39 assessing sensitivity to climate is to measure and analyse spatial variation in tropical ecosystems  
40 across climate gradients as a space-for-time substitution. Such biome-wide spatial variation in forest

41 carbon stocks, fluxes and persistence offers a unique and largely unexplored window into the potential  
42 equilibrium sensitivity of tropical forest vegetation to warming, as it captures real-world vegetation  
43 responses that allow for physiological and ecological adaptation (12).

44 To assess the long-term climate controls on tropical forest growth and carbon stocks, here we have  
45 assembled, measured, and analysed a pan-tropical network of 590 permanent, long-term inventory  
46 plots (Fig. 1, see Figs. S1-2 for ability to capture biome climate space). Our analysis combines  
47 standardised measurements from across South American, African, Asian and Australian tropical  
48 lowland forests (273, 239, 61 and 17 plots respectively). For every plot we calculated aboveground  
49 carbon stocks (19). Then, to better assess the dynamic controls on aboveground carbon stocks, we  
50 also computed the rate of carbon gained by the system (aboveground woody carbon production,  
51 calculated as tree growth plus newly recruited trees, in  $\text{Mg C ha}^{-1} \text{ yr}^{-1}$ ), and its longevity in living  
52 biomass (carbon residence time, calculated as the ratio of stocks to gains, in years).

53 We find considerable variation in biomass carbon among continents, with lower stocks per unit area  
54 in South America compared with the Paleotropics even after accounting for environmental variables  
55 (Fig. 1). Continents with high carbon stocks had either large carbon gains (Asia), or long carbon  
56 residence times (Africa, Fig. 1). Because of these differences among continents, which are potentially  
57 due to differences in evolutionary history (20), we analyse the environmental drivers of spatial  
58 variation in carbon stocks while accounting for biogeographical differences. We fitted linear models  
59 with explanatory variables representing hypothesised mechanistic controls of climate on tropical  
60 forest carbon (Table S1). We also included soil covariates, continent intercepts and eigenvectors  
61 describing spatial relationships amongst plots to account for other sources of variation (21).

62 Forest carbon stocks were most strongly related to maximum temperature ( $-5.9\%$  per  $1^\circ\text{C}$  increase in  
63 maximum temperature, 95 % CI =  $-8.6$  to  $-3.1\%$ , Fig. 2, equivalent to  $9.1 \text{ Mg C ha}^{-1} \text{ }^\circ\text{C}^{-1}$  for a stand  
64 with the mean carbon stocks in our dataset,  $154.6 \text{ Mg C ha}^{-1}$ ), followed by rainfall ( $+2.4\%$  per 100  
65 mm increase in precipitation in the driest quarter, 95 % CI =  $0.6 - 4.3\%$ , Fig. 2), with no statistically  
66 significant relationship with minimum temperature, wind speed or cloud cover (Fig 2). The effects of  
67 maximum temperature and precipitation are also evident in an analysis considering a wider suite of

68 climate variables than those tied to hypothesised mechanisms (Fig. S3), and in an additional  
69 independent pantropical dataset of 223 single-census plots (for which carbon gains and residence time  
70 cannot be assessed, Fig. S4).

71 The negative effect of maximum temperature on aboveground carbon stocks mainly reflects reduced  
72 carbon gains in hotter forests (-4.0 % per 1°C, 95% CI = -6.2 to -1.8 %, Fig. 2) while the positive  
73 effect of precipitation emerges through longer carbon residence times in wetter forests (3.3 % per 100  
74 mm, 95 % CI = 0.9 – 5.7 %, Fig. 2). Carbon residence time also increased with the proportion of clay  
75 in the soil (Fig. 2). The additive effects of precipitation and temperature on carbon stocks were  
76 modified by an interaction between them ( $\Delta$  AIC = 15.4 comparing full linear model with or without  
77 interaction), with temperature effects more negative when precipitation is low (Fig. S6). The  
78 interaction was through shortening carbon residence time ( $\Delta$  AIC = 11.9) rather than reducing carbon  
79 gains (model without interaction better,  $\Delta$  AIC = 1.4).

80 An alternative analysis using decision tree algorithms (22) also showed maximum temperature and  
81 precipitation to be important (Fig. S7). This decision tree approach, which can capture complex non-  
82 linear relationships (22), indicated potential non-linearity in the relationships between carbon stocks  
83 and both temperature and precipitation, with the positive effect of increasing dry season precipitation  
84 on residence times strengthening when precipitation was low, and the negative effect of maximum  
85 temperature intensifying at high temperatures (Fig. S7).

86 We further investigated non-linearity in the temperature relationship using breakpoint regression  
87 (supported over linear regression based on lower AIC,  $\Delta$  AIC = 15.0), which revealed that above 32.2  
88 °C (95 % CI = 31.7 – 32.6 °C) the relationship between carbon stocks and maximum temperature  
89 became more negative (cooler than breakpoint: -3.8 % °C<sup>-1</sup>, warmer than breakpoint: -14.7 % °C<sup>-1</sup>,  
90 Fig. 3). By partitioning carbon stocks into their production and persistence we find that this non-  
91 linearity reflects changes to carbon residence time ( $\Delta$  AIC = 10.6) rather than gains ( $\Delta$  AIC = 1.7).  
92 Overall, our results thus indicate two separate climate controls on carbon stocks: a negative linear  
93 effect of maximum temperature through reduced carbon gains, and a non-linear negative effect of

94 maximum temperature, ameliorated by high dry-season precipitation, through reduced carbon  
95 residence time.

96 The effect of temperature on carbon residence time only emerges when dry season precipitation is  
97 low, so is consistent with theoretical expectations that negative effects of temperature on tree  
98 longevity are exacerbated by moisture limitation rather than being independent of it (i.e. due to  
99 increased respiration costs alone) (23). This could occur through high vapour pressure deficits in hot  
100 and dry forests increasing mortality risk by causing hydraulic stress (23, 24), or carbon starvation due  
101 to limited photosynthesis as a result of stomatal closure (23). Notably, the temperature-precipitation  
102 interaction we find for aboveground stocks is in the opposite direction to temperature-precipitation  
103 interactions reported for soil carbon. In soils, moisture limitation suppresses the temperature response  
104 of heterotrophic respiration (25), while in trees moisture limitation enhances the mortality risks of  
105 high temperatures.

106 The temperature effects on biomass carbon stocks and gains are primarily due to maximum rather  
107 than minimum temperature. This is consistent with high daytime temperatures reducing CO<sub>2</sub>  
108 assimilation rates, for example due to increased photorespiration or longer duration of stomatal  
109 closure (26, 27), whereas if negative temperature effects were to have increased respiration rates there  
110 should be a stronger relationship with minimum (i.e. night-time) temperature. Critically, minimum  
111 temperature is unrelated to aboveground carbon stocks both pan-tropically and in the one continent,  
112 South America, where maximum and minimum temperature are largely decoupled ( $r = 0.33$ ; Fig. S8).  
113 While carbon gains are negatively related to minimum temperature (Fig S9) this bivariate relationship  
114 is weaker than with maximum temperature, and disappears once the effects of other variables are  
115 accounted for (Fig. 2). Finally, in Asia, the tropical region which experiences the warmest minimum  
116 temperatures of all, both carbon stocks and carbon gains are highest (Fig. 1, Fig. S11).

117 Overall our results suggest that tropical forests have considerable potential to acclimate and adapt to  
118 the effects of night-time minimum temperatures, but are clearly sensitive to the effects of daytime  
119 maximum temperature. This is consistent with ecophysiological observations suggesting that the  
120 acclimation potential of respiration (15) is greater than that of photosynthesis (17). The temperature

121 sensitivity revealed by our analysis is also considerably weaker than the short-term sensitivities  
122 associated with inter-annual climate variation (8). For example, by relating short-term annual climate  
123 anomalies to responses in plots, the effect of a 1°C increase in temperature on carbon gains has been  
124 estimated as more than three-fold our long-term, pantropical result (28). This stronger long-term  
125 thermal resilience is likely due to a combination of individual acclimation and plasticity (15-17),  
126 differences in species' climate responses (29) leading to shifts in community composition due to  
127 changing demographic rates (12) and the immigration of species with higher performance at high  
128 temperatures (12).

129 Our pantropical analysis of the sensitivity to climate of aboveground carbon stocks, gains and  
130 persistence shows that warming reduces carbon stocks and gains from woody productivity in tropical  
131 forests. Using a reference carbon stock map (30) and applying our estimated temperature sensitivity  
132 (including non-linearity) while holding other variables constant leads to a biome-wide reduction of  
133 14.1 Pg C in live biomass (including scaling to estimate carbon in roots) for a 1°C increase in  
134 maximum temperature (95 % CI = 6.9 – 20.7 Pg). In comparison, coupled climate-carbon cycle  
135 models (2) give a median tropical land temperature sensitivity of 53 Pg C °C<sup>-1</sup> (95 % CI = 19.7 – 86.3  
136 Pg), although these also incorporate the response of heterotrophic respiration and fire. In the future,  
137 reporting Earth System Model outputs for live biomass carbon separate from other changes would  
138 assist in comparing model outcomes with direct observations.

139 Our results suggest that global surface temperature increases of 2°C above pre-industrial levels will  
140 cause a potential biome-wide loss of 35.3 Pg C (95 % CI = 20.9 – 49.0 Pg) based on responses to  
141 warming from the 1970-2000 baseline (31). The greatest reductions in carbon stocks are projected in  
142 South America, where baseline temperatures and future warming are both highest (Fig. 4, Fig. S12).  
143 This warming would push 71 % of the biome beyond the thermal threshold – maximum temperature  
144 of 32.2°C – where larger reductions in biomass are expected. Of course, growth stimulation by carbon  
145 dioxide (32) will partially or wholly offset the effect of this temperature increase, depending on both  
146 the level of atmospheric carbon dioxide that limits warming to 2°C above pre-industrial levels and the  
147 fertilization effect of this carbon dioxide on tropical trees. Using a variety of published estimates of

148 the carbon dioxide fertilization effect (Table S3), partial or full amelioration is expected in the  
149 Paleotropics, although reductions in forest carbon stocks are predicted in South America in all  
150 scenarios (Fig. S15).

151 The long-term climate sensitivities derived from our pan-tropical field measurements incorporate  
152 ecophysiological and ecological adaptation, and so provide a model-independent estimate of the long-  
153 term quasi-equilibrium response of tropical vegetation to climate, which can inform long-term model  
154 predictions (33). We note that the thermal adaptation measured here may not be fully realised because  
155 (i) the speed of temperature rises may exceed species' adaptive capabilities, (ii) habitat fragmentation  
156 may limit species' ability to track changes in the environment, and (iii) other human impacts such as  
157 logging and fire can increase the vulnerability of forest carbon stocks to high temperatures.

158 Predictions based on short-term inter-annual sensitivity and our long-term pan-tropical sensitivity  
159 likely represent the upper and lower bounds of transient responses to rising temperatures over the  
160 coming decades. While many tropical forests are under severe threat of conversion, our results show  
161 that, in the long-run, tropical forests that remain intact can continue to store high levels of carbon  
162 under high temperatures. Achieving the biome-wide climate resilience potential we document  
163 depends on limiting heating and on large-scale conservation and restoration to protect biodiversity and  
164 allow species to move.

165

166

167 **References and Notes**

- 168 1. P. M. Cox, R. A. Betts, C. D. Jones, S. A. Spall, I. J. Totterdell, Acceleration of global warming  
169 due to carbon-cycle feedbacks in a coupled climate model. *Nature* **408**, 184 (2000).
- 170 2. P. M. Cox *et al.*, Sensitivity of tropical carbon to climate change constrained by carbon  
171 dioxide variability. *Nature* **494**, 341-344 (2013).
- 172 3. B. B. Booth *et al.*, High sensitivity of future global warming to land carbon cycle processes.  
173 *Environmental Research Letters* **7**, 024002 (2012).
- 174 4. K.-H. Erb *et al.*, Unexpectedly large impact of forest management and grazing on global  
175 vegetation biomass. *Nature* **553**, 73 (2017).
- 176 5. W. Wang *et al.*, Variations in atmospheric CO<sub>2</sub> growth rates coupled with tropical  
177 temperature. *Proceedings of the National Academy of Sciences* **110**, 13061 (2013).
- 178 6. J. Liu *et al.*, Contrasting carbon cycle responses of the tropical continents to the 2015–2016  
179 El Niño. *Science* **358**, eaam5690 (2017).
- 180 7. D. A. Clark, S. C. Piper, C. D. Keeling, D. B. Clark, Tropical rain forest tree growth and  
181 atmospheric carbon dynamics linked to interannual temperature variation during 1984–  
182 2000. *Proceedings of the National Academy of Sciences* **100**, 5852 (2003).
- 183 8. W. R. L. Anderegg *et al.*, Tropical nighttime warming as a dominant driver of variability in the  
184 terrestrial carbon sink. *Proceedings of the National Academy of Sciences* **112**, 15591-15596  
185 (2015).
- 186 9. A. Ballantyne *et al.*, Accelerating net terrestrial carbon uptake during the warming hiatus  
187 due to reduced respiration. *Nature Climate Change* **7**, 148 (2017).
- 188 10. J. K. Green *et al.*, Large influence of soil moisture on long-term terrestrial carbon uptake.  
189 *Nature* **565**, 476-479 (2019).
- 190 11. O. L. Phillips *et al.*, Drought Sensitivity of the Amazon Rainforest. *Science* **323**, 1344 (2009).

- 191 12. M. D. Smith, A. K. Knapp, S. L. Collins, A framework for assessing ecosystem dynamics in  
192 response to chronic resource alterations induced by global change. *Ecology* **90**, 3279-3289  
193 (2009).
- 194 13. J. H. Brown, T. J. Valone, C. G. Curtin, Reorganization of an arid ecosystem in response to  
195 recent climate change. *Proceedings of the National Academy of Sciences* **94**, 9729-9733  
196 (1997).
- 197 14. S. Fauset *et al.*, Drought-induced shifts in the floristic and functional composition of tropical  
198 forests in Ghana. *Ecology Letters* **15**, 1120-1129 (2012).
- 199 15. A. Gunderson Carla, H. O'Hara Keiran, M. Campion Christina, V. Walker Ashley, T. Edwards  
200 Nelson, Thermal plasticity of photosynthesis: the role of acclimation in forest responses to a  
201 warming climate. *Global Change Biology* **16**, 2272-2286 (2010).
- 202 16. M. Slot *et al.*, Thermal acclimation of leaf respiration of tropical trees and lianas: response to  
203 experimental canopy warming, and consequences for tropical forest carbon balance. *Global*  
204 *Change Biology* **20**, 2915-2926 (2014).
- 205 17. F. Ow Lai, L. Griffin Kevin, D. Whitehead, S. Walcroft Adrian, H. Turnbull Matthew, Thermal  
206 acclimation of leaf respiration but not photosynthesis in *Populus deltoides* × *nigra*. *New*  
207 *Phytologist* **178**, 123-134 (2008).
- 208 18. T. F. Domingues *et al.*, Ecophysiological plasticity of Amazonian trees to long-term drought.  
209 *Oecologia* **187**, 933-940 (2018).
- 210 19. See suplimentary materials.
- 211 20. J. W. F. Slik *et al.*, Phylogenetic classification of the world's tropical forests. *Proceedings of*  
212 *the National Academy of Sciences* **115**, 1837 (2018).
- 213 21. S. Dray, P. Legendre, P. R. Peres-Neto, Spatial modelling: a comprehensive framework for  
214 principal coordinate analysis of neighbour matrices (PCNM). *Ecological Modelling* **196**, 483-  
215 493 (2006).
- 216 22. L. Breiman, Random Forests. *Machine Learning* **45**, 5-32 (2001).



- 217 23. N. McDowell *et al.*, Drivers and mechanisms of tree mortality in moist tropical forests. *New*  
218 *Phytologist* **219**, 851-869 (2018).
- 219 24. G. Fontes Clarissa *et al.*, Dry and hot: the hydraulic consequences of a climate change–type  
220 drought for Amazonian trees. *Philosophical Transactions of the Royal Society B: Biological*  
221 *Sciences* **373**, 20180209 (2018).
- 222 25. P. Ciais *et al.*, Europe-wide reduction in primary productivity caused by the heat and drought  
223 in 2003. *Nature* **437**, 529-533 (2005).
- 224 26. M. E. Dusenage, A. G. Duarte, D. A. Way, Plant carbon metabolism and climate change:  
225 elevated CO<sub>2</sub> and temperature impacts on photosynthesis, photorespiration and respiration.  
226 *New Phytologist* **221**, 32-49 (2019).
- 227 27. S. Pau, M. Detto, Y. Kim, C. J. Still, Tropical forest temperature thresholds for gross primary  
228 productivity. *Ecosphere* **9**, e02311 (2018).
- 229 28. D. A. Clark, D. B. Clark, S. F. Oberbauer, Field-quantified responses of tropical rainforest  
230 aboveground productivity to increasing CO<sub>2</sub> and climatic stress, 1997-2009. *Journal of*  
231 *Geophysical Research - Biogeosciences*. **118**, 783-794 (2013).
- 232 29. W. R. L. Anderegg *et al.*, Hydraulic diversity of forests regulates ecosystem resilience during  
233 drought. *Nature* **561**, 538-541 (2018).
- 234 30. V. Avitabile *et al.*, An integrated pan-tropical biomass map using multiple reference datasets.  
235 *Global Change Biology* **22**, 1406-1420 (2016).
- 236 31. S. E. Fick, R. J. Hijmans, WorldClim 2: new 1-km spatial resolution climate surfaces for global  
237 land areas. *International Journal of Climatology* **37**, 4302-4315 (2017).
- 238 32. S. Piao *et al.*, Evaluation of terrestrial carbon cycle models for their response to climate  
239 variability and to CO<sub>2</sub> trends. *Global Change Biology* **19**, 2117-2132 (2013).
- 240 33. L. M. Mercado *et al.*, Large sensitivity in land carbon storage due to geographical and  
241 temporal variation in the thermal response of photosynthetic capacity. *New Phytologist* **218**,  
242 1462-1477 (2018).

243 Additional references cited in supplementary materials

- 244 34. A. B. Anderson, White-sand vegetation of Brazilian Amazonia. *Biotropica* **13**, 199-210 (1981).
- 245 35. S. R. Pezeshki, Root responses of flood-tolerant and flood-sensitive tree species to soil redox  
246 conditions. *Trees* **5**, 180-186 (1991).
- 247 36. O. L. Phillips, T. R. Baker, T. R. Feldpausch, R. J. W. Brienen, *RAINFOR Field Manual for Plot*  
248 *Establishment and Remeasurement* (University of Leeds, 2001).
- 249 37. J. Talbot *et al.*, Methods to estimate aboveground wood productivity from long-term forest  
250 inventory plots. *Forest Ecology and Management* **320**, 30-38 (2014).
- 251 38. D. B. Clark, D. A. Clark, Landscape-scale variation in forest structure and biomass in a tropical  
252 rain forest. *Forest Ecology and Management* **137**, 185-198 (2000).
- 253 39. G. Lopez-Gonzalez, S. L. Lewis, M. Burkitt, O. L. Phillips, ForestPlots.net: a web application  
254 and research tool to manage and analyse tropical forest plot data. *Journal of Vegetation*  
255 *Science* **22**, 610-613 (2011).
- 256 40. G. Lopez-Gonzalez, S. L. Lewis, M. Burkitt, T. R. Baker, O. L. Phillips, ForestPlots.net Database.  
257 [www.forestplots.net](http://www.forestplots.net). (2009).
- 258 41. R. J. W. Brienen *et al.*, Long-term decline of the Amazon carbon sink. *Nature* **519**, 344-348  
259 (2015).
- 260 42. J. Chave *et al.*, Improved allometric models to estimate the aboveground biomass of tropical  
261 trees. *Global Change Biology* **20**, 3177-3190 (2014).
- 262 43. J. Chave *et al.*, Towards a worldwide wood economics spectrum. *Ecology Letters* **12**, 351-366  
263 (2009).
- 264 44. A. E. Zanne *et al.* Data from: Towards a worldwide wood economics spectrum.  
265 <https://datadryad.org/stash/dataset/doi:10.5061/dryad.234> (Dryad Data Repository, 2009).
- 266 45. R. C. Goodman *et al.*, Amazon palm biomass and allometry. *Forest Ecology and Management*  
267 **310**, 994-1004 (2013).

- 268 46. M. J. P. Sullivan *et al.*, Field methods for sampling tree height for tropical forest biomass  
269 estimation. *Methods in Ecology and Evolution* **9**, 1179-1189 (2018).
- 270 47. S. C. Thomas, Asymptotic height as a predictor of growth and allometric characteristics in  
271 malaysian rain forest trees. *American Journal of Botany* **83**, 556-566 (1996).
- 272 48. T. R. Feldpausch *et al.*, Tree height integrated into pantropical forest biomass estimates.  
273 *Biogeosciences* **9**, 3381-3403 (2012).
- 274 49. T. S. Kohyama, T. I. Kohyama, D. Sheil, Definition and estimation of vital rates from repeated  
275 censuses: Choices, comparisons and bias corrections focusing on trees. *Methods in Ecology*  
276 *and Evolution* **9**, 809-821 (2018).
- 277 50. A. R. Martin, M. Doraisami, S. C. Thomas, Global patterns in wood carbon concentration  
278 across the world's trees and forests. *Nature Geoscience* **11**, 915-920 (2018).
- 279 51. D. Galbraith *et al.*, Residence times of woody biomass in tropical forests. *Plant Ecology &*  
280 *Diversity* **6**, 139-157 (2013).
- 281 52. G. Lopez-Gonzalez, M. J. P. Sullivan, T. R. Baker. BiomasaFP: R package for analysing data  
282 downloaded from ForestPlots.net (2015).
- 283 53. R. J. Hijmans, S. Phillips, J. Leathwick, J. Elith, dismo: Species distribution modeling. R  
284 package version 1.0-12. (2015).
- 285 54. A. M. Wilson, W. Jetz, Remotely Sensed High-Resolution Global Cloud Dynamics for  
286 Predicting Ecosystem and Biodiversity Distributions. *PLOS Biology* **14**, e1002415 (2016).
- 287 55. M. New, D. Lister, M. Hulme, I. Makin, A high-resolution data set of surface climate over  
288 global land areas. *Climate Research* **21**, 1-25 (2002).
- 289 56. T. Hengl *et al.*, SoilGrids250m: Global gridded soil information based on machine learning.  
290 *PLOS ONE* **12**, e0169748 (2017).
- 291 57. P. R. Peres-Neto, P. Legendre, Estimating and controlling for spatial structure in the study of  
292 ecological communities. *Global Ecology and Biogeography* **19**, 174-184 (2010).

- 293 58. S. L. Lewis *et al.*, Increasing carbon storage in intact African tropical forests. *Nature* **457**,  
294 1003 (2009).
- 295 59. K. Barton, MuMIn: Multi-Model Inference. R package version 1.12.1. [http://CRAN.R-](http://CRAN.R-project.org/package=MuMIn)  
296 [project.org/package=MuMIn](http://CRAN.R-project.org/package=MuMIn) (2015).
- 297 60. V. M. R. Muggeo, Estimating regression models with unknown break-points. *Statistics in*  
298 *Medicine* **22**, 3055-3071 (2003).
- 299 61. A. Liaw, M. Wiener, Classification and Regression by randomForest. *R News* **2**, 18-22 (2002).
- 300 62. D. M. Olson *et al.*, Terrestrial Ecoregions of the World: A New Map of Life on Earth A new  
301 global map of terrestrial ecoregions provides an innovative tool for conserving biodiversity.  
302 *BioScience* **51**, 933-938 (2001).
- 303 63. M. C. Hansen *et al.*, High-Resolution Global Maps of 21st-Century Forest Cover Change.  
304 *Science* **342**, 850-853 (2013).
- 305 64. R. Jackson *et al.*, A global analysis of root distributions for terrestrial biomes. *Oecologia* **108**,  
306 389-411 (1996).
- 307 65. S. S. Saatchi *et al.*, Benchmark map of forest carbon stocks in tropical regions across three  
308 continents. *Proceedings of the National Academy of Sciences* **108**, 9899-9904 (2011).
- 309 66. A. Baccini *et al.*, Estimated carbon dioxide emissions from tropical deforestation improved  
310 by carbon-density maps. *Nature Climate Change* **2**, 182-185 (2012).
- 311 67. E. T. A. Mitchard *et al.*, Uncertainty in the spatial distribution of tropical forest biomass: a  
312 comparison of pan-tropical maps. *Carbon Balance and Management* **8**, 10 (2013).
- 313 68. E. T. Mitchard *et al.*, Markedly divergent estimates of Amazon forest carbon density from  
314 ground plots and satellites. *Global Ecology and Biogeography* **23**, 935-946 (2014).
- 315 69. R. J. Hijmans. WorldClim Future Climate Data <https://www.worldclim.org/cmip5v1>. (2005).
- 316 70. R. J. Hijmans, S. E. Cameron, J. L. Parra, P. G. Jones, A. Jarvis, Very high resolution  
317 interpolated climate surfaces for global land areas. *International Journal of Climatology* **25**,  
318 1965-1978 (2005).

- 319 71. B. Kirtman *et al.*, Near-term climate change: projections and predictability. (2013).
- 320 72. H. D. Matthews, K. Caldeira, Stabilizing climate requires near-zero emissions. *Geophysical*  
321 *Research Letters* **35**, (2008).
- 322 73. M. Meinshausen *et al.*, The RCP greenhouse gas concentrations and their extensions from  
323 1765 to 2300. *Climatic Change* **109**, 213 (2011).
- 324 74. W. Kolby Smith *et al.*, Large divergence of satellite and Earth system model estimates of  
325 global terrestrial CO<sub>2</sub> fertilization. *Nature Climate Change* **6**, 306 (2015).
- 326 75. D. W. Kicklighter *et al.*, A first-order analysis of the potential role of CO<sub>2</sub> fertilization to affect  
327 the global carbon budget: a comparison of four terrestrial biosphere models. *Tellus B:*  
328 *Chemical and Physical Meteorology* **51**, 343-366 (1999).
- 329 76. Y. Malhi *et al.*, The linkages between photosynthesis, productivity, growth and biomass in  
330 lowland Amazonian forests. *Global Change Biology* **21**, 2283-2295 (2015).
- 331 77. C. Terrer *et al.*, Nitrogen and phosphorus constrain the CO<sub>2</sub> fertilization of global plant  
332 biomass. *Nature Climate Change* **9**, 684-689 (2019).
- 333 78. E. Bartholome, A. S. Belward, GLC2000: a new approach to global land cover mapping from  
334 Earth observation data. *International Journal of Remote Sensing* **26**, 1959-1977 (2005).
- 335 79. J. Chave *et al.*, Tree allometry and improved estimation of carbon stocks and balance in  
336 tropical forests. *Oecologia* **145**, 87-99 (2005).
- 337 80. M. Slot, K. Winter, In situ temperature response of photosynthesis of 42 tree and liana  
338 species in the canopy of two Panamanian lowland tropical forests with contrasting rainfall  
339 regimes. *New Phytologist* **214**, 1103-1117 (2017).
- 340 81. Y. Malhi, The productivity, metabolism and carbon cycle of tropical forest vegetation.  
341 *Journal of Ecology* **100**, 65-75 (2012).
- 342 82. E. A. Graham, S. S. Mulkey, K. Kitajima, N. G. Phillips, S. J. Wright, Cloud cover limits net CO<sub>2</sub>  
343 uptake and growth of a rainforest tree during tropical rainy seasons. *Proceedings of the*  
344 *National Academy of Sciences* **100**, 572-576 (2003).

- 345 83. W. F. Laurance, T. J. Curran, Impacts of wind disturbance on fragmented tropical forests: A  
 346 review and synthesis. *Austral Ecology* **33**, 399-408 (2008).

347 **Acknowledgements:** This paper is a product of the RAINFOR, AfriTRON and T-FORCES networks,  
 348 and is facilitated by ForestPlots.net technology for data management which promotes science  
 349 synergies across countries and continents. While these initiatives have been supported by numerous  
 350 people and grants since their inception we are particularly indebted to hundreds of institutions, field  
 351 assistants and local communities for help in establishing and maintaining the plots. For additional  
 352 assistance with access to datasets we thank Jon Lloyd, Carlos Quesada, Michel Baisie, Olaf Banki,  
 353 Wemo Betian, Vincent Bezar, Rene Boot, Mireille Breuer-Ndoundou Hockemba, Ezequiel Chavez,  
 354 Douglas Daly, Armandu Daniels, Darcy Galiano Cabrera, Toby Gardner, Paolo Graca, Andrew  
 355 Graham, Olivier Hardy, Eduardo Hase, David Hilvert, Muhammad Idhamsyah, Phillipe Jeanmart,  
 356 Cisquet Keibou Opepa, Jeanette Kemp, Wilmar Lopez Oviedo, Jean-Remy Makana, Faustin Mbaya  
 357 Mpanya Lukasu, Irina Mendoza Polo, Edi Mirmanto, Sam Moore, Jacques Mukinzi, Pétrus Naisso,  
 358 Lucas Ojo, Raimunda Oliveira de Araújo, Sonia Cesarina Palacios Ramos, Alexander Parada  
 359 Gutierrez, Guido Pardo, Marielos Peña-Claros, Freddy Ramirez Arevalo, Antonio Lima, Rodrigo  
 360 Sierra, Natalino Silva, Marc Steininger, Marisol Toledo, John Tshibamba Mukendi, Darlington  
 361 Tuagben, Hannsjoerg Woell and Ishak Yassir. We thank Jon Lloyd, Carlos Quesada for discussions  
 362 and three anonymous reviewers for helpful comments and suggestions. **Funding:** The networks have  
 363 been supported by multiple grants, most notably the European Research Council (ERC Advanced  
 364 Grant 291585 – ‘T-FORCES’), the Gordon and Betty Moore Foundation (#1656 ‘RAINFOR’ and  
 365 Monitoring Protected Areas in Peru to Increase Forest Resilience to Climate Change), the David and  
 366 Lucile Packard Foundation, the European Union’s Seventh Framework Programme (283080 –  
 367 ‘GEOCARBON’, 282664 – ‘AMAZALERT’), the Natural Environment Research Council (NERC  
 368 grants NE/D005590/1 – ‘TROBIT’, NE/F005806/1 – ‘AMAZONICA’, NERC Urgency Grants and a  
 369 NERC New Investigators Grant), the NERC/ State of São Paulo Research Foundation (FAPESP)  
 370 consortium grants ‘BIO-RED’ (NE/N012542/1, 2012/51872-5) and ‘ECOFOR’ (NE/K016431/1,  
 371 2012/51509-8), the Royal Society, the Centre for International Forestry (CIFOR) and Gabon’s  
 372 National Parks Agency (ANPN). Additional data were included from the Tropical Ecology  
 373 Assessment and Monitoring (TEAM) Network, a collaboration between Conservation International,  
 374 the Missouri Botanical Garden, the Smithsonian Institution and the Wildlife Conservation Society,  
 375 and partly funded by these institutions, the Gordon and Betty Moore Foundation, and other donors.  
 376 M.J.P.S. was supported by the ERC (T-FORCES), NERC (‘BIO-RED’) and the Royal Society  
 377 (CH160091), S.L.L. by a Royal Society University Research Fellowship, ERC Advanced Grant and a  
 378 Phillip Leverhulme Prize, and O.L.P. by an ERC Advanced Grant and a Royal Society Wolfson  
 379 Research Merit Award. We thank the National Council for Science and Technology Development of  
 380 Brazil (CNPq) for support to the Cerrado/Amazonia Transition Long-Term Ecology Project  
 381 (PELD/403725/2012-7), the PPBio Phytogeography of Amazonia/Cerrado Transition project  
 382 (CNPq/PPBio/457602/2012-0) and a Productivity Grant to B.S.M. and B.H.M-J.. Funding for plots in  
 383 the Udzungwa Mountains (Tanzania) was obtained from the Leverhulme Trust under the Valuing the  
 384 Arc project. This study is contribution number XXX to the Technical Series (TS) of the BDFFP  
 385 (INPA – STRI). Data from RAINFOR, AfriTRON and T-FORCES are stored and curated by  
 386 ForestPlots.net, a cyber-infrastructure initiative hosted at the University of Leeds that unites  
 387 permanent plot records and their contributing scientists from the world’s tropical forests. The  
 388 development of ForestPlots.net and curation of most data analysed here was funded by several grants  
 389 to O.L.P. (principally from NERC NE/B503384/1, NE/N012542/1 BIO-RED, ERC AdG 291585 T-  
 390 FORCES’, and Gordon and Betty Moore Foundation #1656, ‘RAINFOR’), E.G. (‘GEOCARBON’,  
 391 and NE/F005806/1 ‘AMAZONICA’), T.R.B. (Gordon and Betty Moore Foundation ‘Monitoring  
 392 Protected Areas in Peru to Increase Forest Resilience to Climate Change’), S.L.L. (Royal Society

393 University Research Fellowship; NERC New Investigators Award; Phillip Leverhulme Prize), and  
394 D.G. (NERC NE/N004655/1, 'TREMOR'). **Author contributions:** O.L.P., S.L.L. and Y.M.  
395 conceived the RAINFOR, AfriTRON and T-FORCES forest census network programmes; M.J.P.S.,  
396 S.L.L. and O.L.P. conceived and designed the study. L.A., A.A.-M., T.R.B., R.J.W.B., S.K.B., K.A-  
397 B., F.C., C.C., E.A.D., A.C.S., C.E.N.E., T.R.F., W.H., S.L.L., A.M.M., B.S.M., O.L.P., L.Q., B.S.,  
398 T.S., R.V. and L.J.T.W. coordinated data collection with the help of most co-authors. O.L.P., T.R.B.,  
399 G.L.-G. and S.L.L. conceived and managed ForestPlots.net; O.L.P., T.R.B., D.G., E.G. and S.L.L.  
400 funded it, and R.B., T.F., G.L.-G., A.L., G.C.P. and M.J.P.S. helped develop it. M.J.P.S., T.R.B.,  
401 W.H., S.L.L., A.E.-M., and L.Q. contributed tools to analyse data. All authors collected or supported  
402 the collection of field data, M.J.P.S. analysed the data, M.J.P.S., S.L.L. and O.L.P. wrote the  
403 manuscript with contributions from other authors. All co-authors commented on or approved the  
404 manuscript. **Competing interests:** The authors declare no competing financial interests. **Data and**  
405 **materials availability:** Plot-level input data and R scripts will be deposited as a data package on  
406 ForestPlots.net (doi-xxx).

407

408 **Supplementary Materials:**

409 Materials and Methods

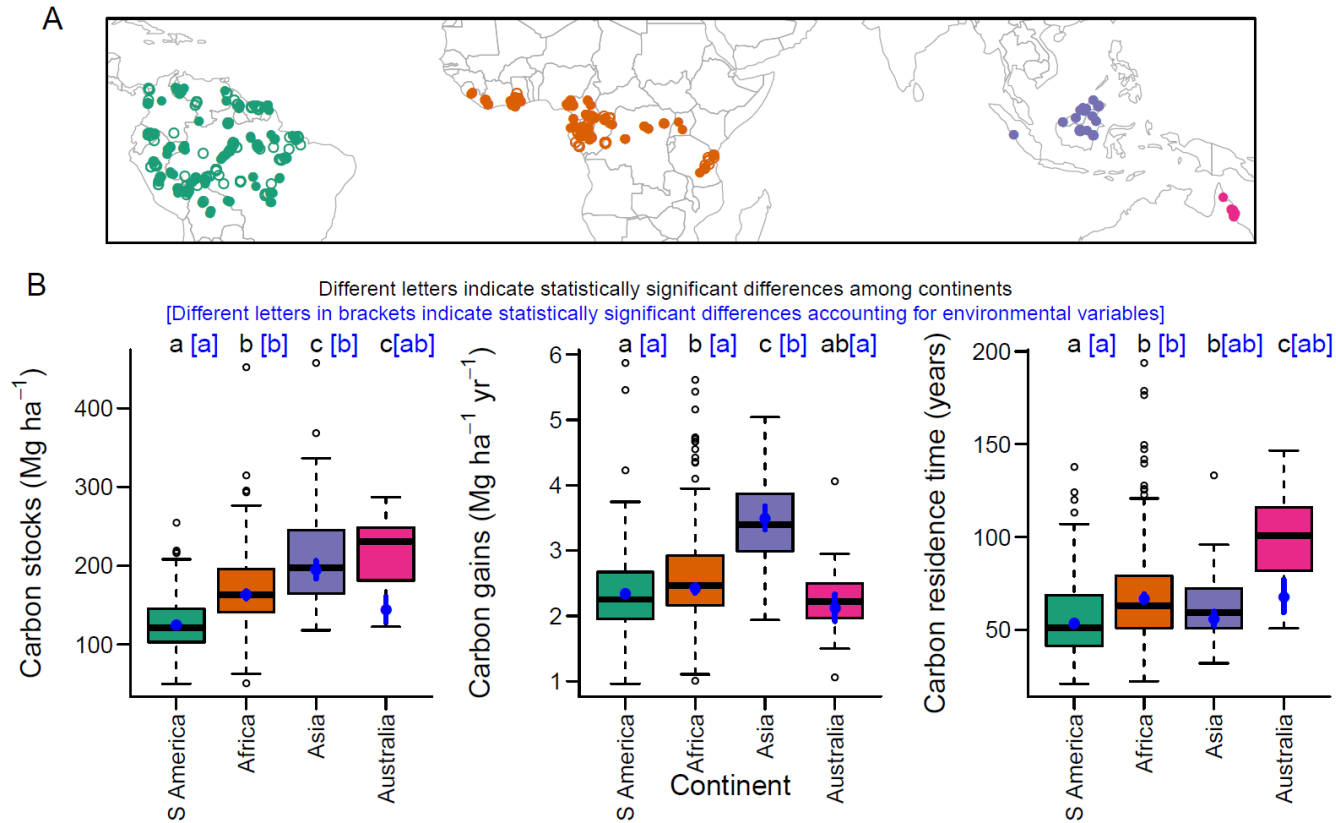
410 Figures S1-S15

411 Tables S1-S3

412 References (34-83)



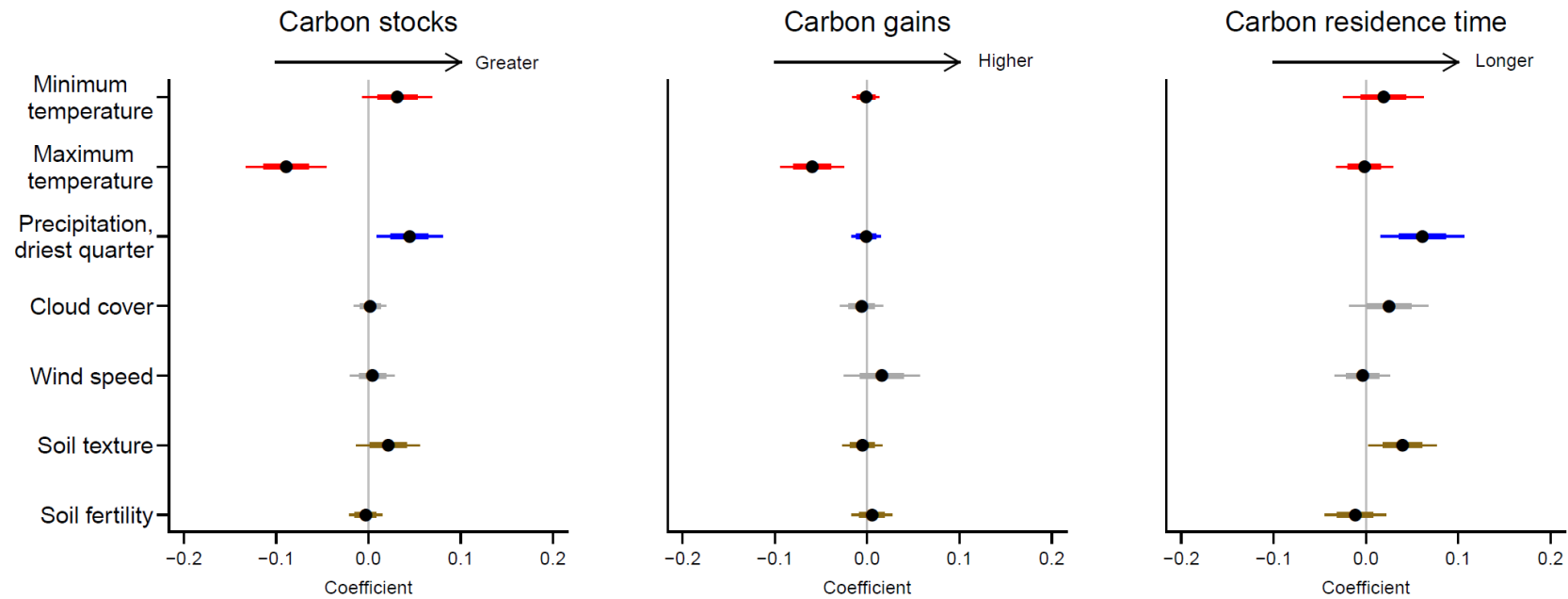
413



414

415 **Figure 1.** Spatial variation in tropical forest carbon. (A) Our plot network. Filled symbols show multi-census plots used in the main analysis, open symbols  
 416 show single-census plots used as an independent dataset. (B) Variation in carbon among continents. Boxplots show raw variation while blue points show  
 417 estimated mean values ( $\pm$  SE) after accounting for environmental variation. Letters denote statistically significant differences between continents ( $P < 0.05$ )  
 418 based on raw data (black) or accounting for environmental effects (blue, square brackets).

419

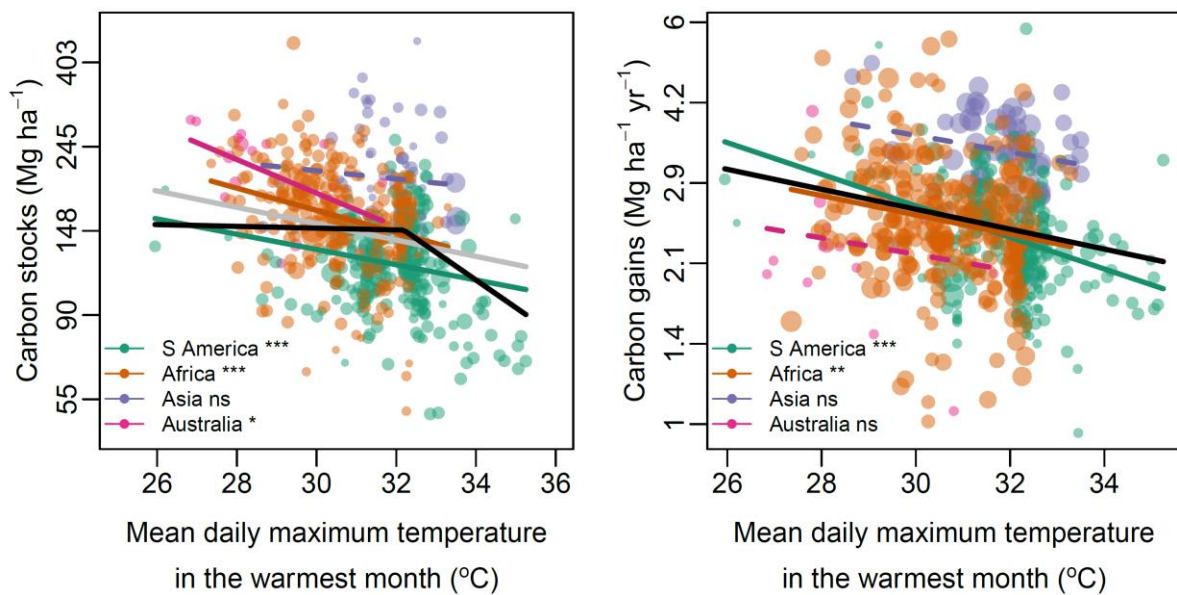


420

421 **Figure 2.** Correlates of spatial variation in tropical forest carbon. Points show coefficients from model-averaged general linear models. Variables that did not  
 422 occur in well-supported models are shrinkage adjusted towards zero. Coefficients are standardised so that they represent change in the response variable for  
 423 one standard deviation change in the explanatory variable. Error bars show standard errors (thick lines) and 95% confidence intervals (thin lines). Soil texture  
 424 is represented by the percentage clay, and soil fertility by cation exchange capacity. The full models explained 44.1 %, 31.4 % and 30.9 % of spatial variation  
 425 in carbon stocks, gains and residence time respectively. Coefficients are shown in Table S2. Results are robust to using an alternative allometry to estimate  
 426 tree biomass (Fig. S5).

427

428



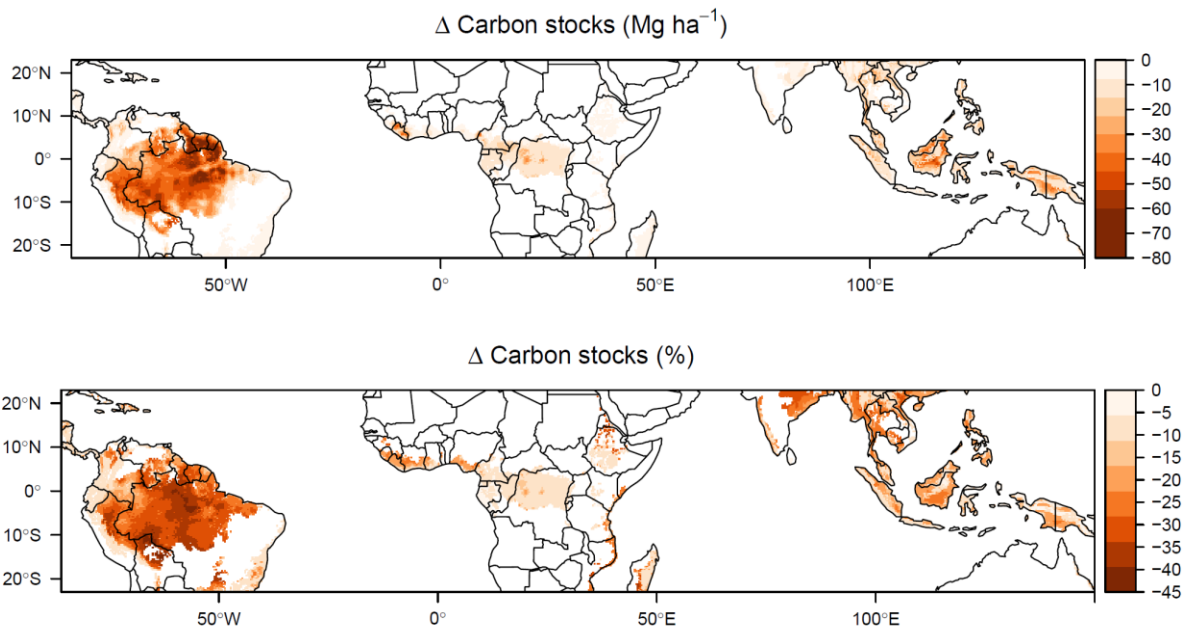
429

430

431 **Figure 3.** Temperature effects on tropical forest carbon stocks (left) and carbon gains from woody  
 432 productivity (right). Black lines show the best pan-tropical relationships accounting for environmental  
 433 covariates. The grey line shows the additional linear pan-tropical relationship for carbon stocks.  
 434 Coloured lines show bivariate relationships within each continent. Statistically significant  
 435 relationships are shown with solid lines, non-significant with dashed lines. Symbol point size is  
 436 proportional to weights used in model fitting based on plot size and monitoring length, see SI  
 437 Materials and Methods. Linear and break-point pan-tropical relationships are all statistically  
 438 significant ( $P < 0.001$ ), as are better sampled continents. Relationships with other variables are shown  
 439 in Fig. S8-S10. \*\*\*  $P < 0.001$ , \*\*  $P < 0.01$ , \*  $P < 0.05$ , ns  $P \geq 0.05$ .

440

441



442

443 **Figure 4.** Long-term change in carbon stocks due to global surface temperature warming of  
444 approximately 2°C. Future temperatures come from an ensemble of 15 climate models for RCP4.5,  
445 2040-2060, which give global mean surface temperatures ~ 1.9°C above pre-industrial. Maps show  
446 the predicted absolute and relative change in tropical forest carbon stocks if global temperatures  
447 equilibrated at these new levels, based on the increase in maximum temperature from 1970-2000  
448 baseline climate. Note parts of the biome become warmer than currently observed in our dataset (Fig.  
449 S13). See Fig. S14 for predictions using alternative carbon reference maps. Predictions are based on  
450 temperature alone and do not include precipitation changes (for which future patterns of change are  
451 uncertain) or potential moderation via elevated CO<sub>2</sub> (see Fig. S15).

452

453

454 **Supporting information for Long-term thermal Sensitivity of the Earth's Tropical**  
 455 **Forests**

456 Martin J. P. Sullivan<sup>1,2</sup>, Simon L. Lewis<sup>1,3</sup>, Kofi Affum-Baffoe<sup>4</sup>, Carolina Castilho<sup>5</sup>, Flávia Costa<sup>6</sup>, Aida  
 457 Cuni Sanchez<sup>7,8</sup>, Corneille E. N. Ewango<sup>9,10,11</sup>, Wannes Hubau<sup>1,12,13</sup>, Beatriz Marimon<sup>14</sup>, Abel Monteagudo-  
 458 Mendoza<sup>15</sup>, Lan Qie<sup>16</sup>, Bonaventure Sonké<sup>17</sup>, Rodolfo Vasquez Martinez<sup>15</sup>, Timothy R Baker<sup>1</sup>, Roel J. W.  
 459 Brien<sup>1</sup>, Ted R. Feldpausch<sup>18</sup>, David Galbraith<sup>1</sup>, Manuel Gloor<sup>1</sup>, Yadvinder Malhi<sup>19</sup>, Shin-Ichiro Aiba<sup>20</sup>,  
 460 Miguel N. Alexiades<sup>21</sup>, Everton C. Almeida<sup>22</sup>, Edmar Almeida de Oliveira<sup>23</sup>, Esteban Álvarez Dávila<sup>24</sup>,  
 461 Patricia Alvarez Loayza<sup>25</sup>, Ana Andrade<sup>26</sup>, Simone Aparecida Vieira<sup>27</sup>, Luiz Aragão<sup>28</sup>, Alejandro Araujo-  
 462 Murakami<sup>29</sup>, Eric J.M.M. Arets<sup>30</sup>, Luzmila Arroyo<sup>31</sup>, Peter Ashton<sup>32</sup>, Gerardo Aymard C.<sup>33</sup>, Fabrício B.  
 463 Baccaro<sup>34</sup>, Lindsay F. Banin<sup>35</sup>, Christopher Baraloto<sup>36</sup>, Plínio Barbosa Camargo<sup>37</sup>, Jos Barlow<sup>38</sup>, Jorcely  
 464 Barroso<sup>39</sup>, Jean-François Bastin<sup>40</sup>, Sarah A. Batterman<sup>1,41,42,43</sup>, Hans Beeckman<sup>12</sup>, Serge K. Begne<sup>17,44</sup>, Amy  
 465 C. Bennett<sup>44</sup>, Erika Berenguer<sup>19,38</sup>, Nicholas Berry<sup>45</sup>, Lilian Blanc<sup>46</sup>, Pascal Boeckx<sup>47</sup>, Jan Bogaert<sup>48</sup>, Damien  
 466 Bonal<sup>49</sup>, Frans Bongers<sup>50</sup>, Matt Bradford<sup>51</sup>, Francis Q. Brearley<sup>2</sup>, Terry Brncic<sup>52</sup>, Foster Brown<sup>53</sup>, Benoit  
 467 Burban<sup>54</sup>, José Luís Camargo<sup>26</sup>, Wendeson Castro<sup>55</sup>, Carlos Céron<sup>56</sup>, Sabina Cerruto Ribeiro<sup>57</sup>, Victor  
 468 Chama Moscoso<sup>15</sup>, Jérôme Chave<sup>58</sup>, Eric Chezeaux<sup>59</sup>, Connie J. Clark<sup>25</sup>, Fernanda Coelho<sup>1</sup>, Murray  
 469 Collins<sup>61</sup>, James A. Comiskey<sup>62,63</sup>, Fernando Cornejo Valverde<sup>64</sup>, Massiel Corrales Medina<sup>65</sup>, Lola da  
 470 Costa<sup>66</sup>, Martin Dančák<sup>67</sup>, Greta C. Dargie<sup>1</sup>, Stuart Davies<sup>68</sup>, Nallaret Davila Cardozo<sup>69</sup>, Thales de  
 471 Haulleville<sup>12,48</sup>, Marcelo Brilhante de Medeiros<sup>70</sup>, Jhon del Aguila Pasquel<sup>71</sup>, Géraldine Derroire<sup>72</sup>, Anthony  
 472 Di Fiore<sup>73</sup>, Jean-Louis Doucet<sup>74</sup>, Aurélie Dourdain<sup>72</sup>, Vincent Droissant<sup>75</sup>, Luisa Fernanda Duque<sup>76</sup>, Romeo  
 473 Ekoungoulou<sup>77</sup>, Fernando Elias<sup>78</sup>, Terry Erwin<sup>79</sup>, Adriane Esquivel-Muelbert<sup>80</sup>, Sophie Fauset<sup>81</sup>, Joice  
 474 Ferreira<sup>82</sup>, Gerardo Flores Llampazo<sup>83</sup>, Ernest Foli<sup>84</sup>, Andrew Ford<sup>51</sup>, Martin Gilpin<sup>1</sup>, Jefferson S. Hall<sup>85</sup>,  
 475 Keith C. Hamer<sup>86</sup>, Alan C. Hamilton<sup>87</sup>, David J. Harris<sup>88</sup>, Terese B. Hart<sup>89,90</sup>, Radim Hédli<sup>91,92</sup>, Bruno  
 476 Hérault<sup>72</sup>, Rafael Herrera<sup>93</sup>, Niro Higuchi<sup>6</sup>, Annette Hladik<sup>94</sup>, Eurídice Honorio Coronado<sup>71</sup>, Isau  
 477 Huamantupa-Chuquimaco<sup>95</sup>, Walter Huaraca Huasco<sup>95</sup>, Kathryn J. Jeffery<sup>96</sup>, Eliana Jimenez-Rojas<sup>97</sup>,  
 478 Michelle Kalamandeen<sup>1</sup>, Marie-Noel Kamdem<sup>11,13,17,98</sup>, Elizabeth Kearsley<sup>99</sup>, Ricardo Keichi Umetsu<sup>100</sup>, Lip  
 479 Khoon Kho Khoon<sup>101</sup>, Timothy Killeen<sup>102</sup>, Kanehiro Kitayama<sup>103</sup>, Bente Klitgaard<sup>104</sup>, Nicolas Labrière<sup>58</sup>,  
 480 William Laurance<sup>105</sup>, Susan Laurance<sup>105</sup>, Miguel E. Leal<sup>106</sup>, Aurora Levesley<sup>1</sup>, Adriano J. N. Lima<sup>6</sup>, Janvier  
 481 Lisingo<sup>11</sup>, Aline P. Lopes<sup>107,108</sup>, Gabriela Lopez-Gonzalez<sup>1</sup>, Tom Lovejoy<sup>109</sup>, Jon Lovett<sup>1</sup>, Richard Lowe<sup>110</sup>,  
 482 William E. Magnusson<sup>111</sup>, Jagoba Malumbres-Olarte<sup>112,113</sup>, Ângelo Gilberto Manzatto<sup>114</sup>, Ben Hur Marimon  
 483 Junior<sup>115</sup>, Andrew R. Marshall<sup>8,116,117</sup>, Toby Marthews<sup>118</sup>, Simone Matias de Almeida Reis<sup>14,19</sup>, Colin  
 484 Maycock<sup>119</sup>, Karina Melgaço<sup>1</sup>, Casimiro Mendoza<sup>120</sup>, Faizah Metali<sup>121</sup>, Vianet Mihindou<sup>122,123</sup>, William  
 485 Milliken<sup>104</sup>, Edward Mitchard<sup>124</sup>, Paulo S. Morandi<sup>14</sup>, Hannah L. Mossman<sup>2</sup>, Laszlo Nagy<sup>125</sup>, Henrique  
 486 Nascimento<sup>6</sup>, David Neill<sup>126</sup>, Reuben Nilus<sup>127</sup>, Percy Núñez Vargas<sup>95</sup>, Walter Palacios<sup>128</sup>, Nadir Pallqui  
 487 Camacho<sup>1,95</sup>, Julie Peacock<sup>1</sup>, Colin Pendry<sup>129</sup>, Maria Cristina Peñuela Mora<sup>130</sup>, Georgia C. Pickavance<sup>1</sup>, John  
 488 Pipoly<sup>131</sup>, Nigel Pitman<sup>132</sup>, Maureen Playfair<sup>133</sup>, Lourens Poorter<sup>134</sup>, John R. Poulsen<sup>25</sup>, Axel D. Poulsen<sup>135</sup>,  
 489 Richard Preziosi<sup>2</sup>, Adriana Prieto<sup>136</sup>, Richard Primack<sup>137</sup>, Hirma Ramírez-Angulo<sup>138</sup>, Jan Reitsma<sup>139</sup>,  
 490 Maxime Réjou-Méchain<sup>75</sup>, Zorayda Restrepo Correa<sup>140</sup>, Thaiane Rodrigues de Sousa<sup>6</sup>, Lily Rodriguez  
 491 Bayona<sup>141</sup>, Anand Roopsind<sup>142</sup>, Agustín Rudas<sup>136</sup>, Ervan Rutishauser<sup>42,143</sup>, Kamariah Abu Salim<sup>121</sup>, Rafael  
 492 P. Salomão<sup>144,145</sup>, Juliana Schiatti<sup>6</sup>, Douglas Sheil<sup>146</sup>, Richarlly C. Silva<sup>57,147</sup>, Javier Silva Espejo<sup>148</sup>, Camila  
 493 Silva Valeria<sup>38</sup>, Marcos Silveira<sup>57</sup>, Murielle Simo-Droissart<sup>17</sup>, Marcelo Fragomeni Simon<sup>70</sup>, James Singh<sup>149</sup>,  
 494 Yahn Carlos Soto Shareva<sup>15</sup>, Clement Stahl<sup>54</sup>, Juliana Stropp<sup>150</sup>, Rahayu Sukri<sup>121</sup>, Terry Sunderland<sup>151,152</sup>,  
 495 Martin Svátek<sup>153</sup>, Michael D. Swaine<sup>154</sup>, Varun Swamy<sup>155</sup>, Hermann Taedoum<sup>17</sup>, Joey Talbot<sup>1</sup>, James  
 496 Taplin<sup>156</sup>, David Taylor<sup>157</sup>, Hans ter Steege<sup>158,159</sup>, John Terborgh<sup>25</sup>, Raquel Thomas<sup>142</sup>, Sean C. Thomas<sup>160</sup>,  
 497 Armando Torres-Lezama<sup>161</sup>, Peter Umunay<sup>162,163</sup>, Luis Valenzuela Gamarra<sup>15</sup>, Geertje van der Heijden<sup>164</sup>,  
 498 Peter van der Hout<sup>165</sup>, Peter van der Meer<sup>166</sup>, Mark van Nieuwstadt<sup>167</sup>, Hans Verbeeck<sup>99</sup>, Ronald  
 499 Vernimmen<sup>168</sup>, Alberto Vicentini<sup>6</sup>, Ima Célia Guimarães Vieira<sup>145</sup>, Emilio Vilanova Torre<sup>169</sup>, Jason  
 500 Vleminckx<sup>36</sup>, Vincent Vos<sup>171</sup>, Ophelia Wang<sup>172</sup>, Lee J. T. White<sup>123,173,174</sup>, Simon Willcock<sup>175</sup>, John T.  
 501 Woods<sup>176</sup>, Verginia Wortel<sup>177</sup>, Kenneth Young<sup>178</sup>, Roderick Zagt<sup>179</sup>, Lise Zemagho<sup>17</sup>, Pieter A. Zuidema<sup>50</sup>,  
 502 Joeri A. Zwarts<sup>177,180</sup>, Oliver L. Phillips<sup>1</sup>

503

504

505 **This file includes:**  
506 Materials and Methods  
507 Figures S1 – S15  
508 Tables S1 – S3  
509

510 **Materials and Methods**

511 Forest census data

512 Our plots come from the RAINFOR, AfriTRON, and T-FORCES networks. Forest inventory plots  
513 were located in lowland (<1200 m), old-growth, closed-canopy forests that were not known to have  
514 been subject to anthropogenic disturbance through fire or selective logging. Plots characterised  
515 floristically as dry forest were not included, as were plots that received less than 1200 mm  
516 precipitation each year. We also did not include plots in white sand, swamp and seasonally flooded  
517 forests, as we expect these to experience marked edaphic constraints (extreme nutrient limitation for  
518 white sand forests (34), stress caused by hypoxic conditions for swamp and seasonally flooded forests  
519 (35)). All plots were  $\geq 0.2$  ha (median size = 1 ha) and were monitored for at least two years (median  
520 monitoring period = 9.7 years). All censuses were prior to the 2015-16 very strong El Niño event, as  
521 we expected that event to suppress carbon gains relative to the long-term mean.

522 Forest inventory plots were sampled using standardised protocols (36), where all live stems with  
523 diameter  $\geq 100$  mm were measured at 1.3 m or 50 cm above buttresses and deformities. Trees were  
524 tagged so that the same tree could be identified in subsequent censuses. In some cases the point of  
525 diameter measurement (POM) had to be moved due to upward growth of buttresses and deformities.  
526 For these trees we use the  $D_{\text{mean}}$  approach from Talbot et al. (37).

527 In a few cases (6 plots) the minimum diameter measured changed over time, or palms and  
528 *Phenakospermum* were excluded in some censuses. For these, we estimated aboveground biomass  
529 (AGB, subsequently converted to carbon stocks) and aboveground woody production (AGWP,  
530 subsequently converted to carbon gains) using a minimum diameter or taxonomic protocol that could  
531 be consistently applied across censuses, and scaled these values by the aboveground biomass ratio  
532 between that protocol and all stems  $\geq 100$  mm protocol for censuses when all stems were measured.  
533 Some plots had nested designs where the plot was split into subplots with different minimum diameter  
534 protocols (69 plots). For these, we only analysed the area conforming to our minimum diameter  
535 protocol. For analysis, we grouped small ( $\leq 0.5$  ha) plots within 1 km of each other, and also grouped

536 contiguous larger plots (18 plots), as these will experience equivalent climate and larger plots are less  
537 sensitive to stochastic tree fall events (38).

538 Data were curated in ForestPlots.net (39, 40), or were subject to equivalent offline handling, and  
539 experienced the same quality control procedures. Details of quality control procedures are described  
540 in Brien et al. (41). Our final dataset consists of 590 sampling units (hereafter plots) covering 637.2  
541 ha, with 2.2 million measurements of 670,499 unique stems. For validating models of carbon stocks  
542 an additional dataset of 223 single-census plots using the same measurement protocols was assembled  
543 from the same networks (see section “Validation with independent single-census plot dataset” below).

544

#### 545 Estimating above-ground biomass

546 Diameter measurements were converted to estimates of aboveground biomass (AGB). For dicot trees  
547 we used the allometric equation

$$548 \text{ AGB} = 0.673 \times (\rho D^2 H)^{0.976}, \quad [1]$$

549 from Chave et al. (42), where  $\rho$  is wood density (from (43, 44)) and  $H$  is tree height estimated using  
550 allometric equations described below. For monocots and tree ferns, we used a palm-specific  
551 allometric equation

$$552 \ln(\text{AGB}) = -3.3488 + 2.7483 \ln(D), \quad [2]$$

553 from Goodman et al. (45), where  $D$  is the measured diameter.

554 The heights of a subset of trees in our dataset were measured in the field, either with a laser  
555 rangefinder, hypsometer, or clinometer, or directly by climbing the tree. We filtered this dataset to  
556 stems with measured diameters, height  $\leq 90$  m, diameters  $\geq 90$  mm DBH, as height-diameter  
557 allometries of saplings differ from those of more mature trees, and to stems that were not broken,  
558 leaning or fallen. This gave a total of 78,899 height measurements. We used this dataset to fit local  
559 height-diameter allometric models, as these refine AGB estimates by capturing spatial variation in  
560 height-diameter allometries missed by large-scale allometric models (46). Height data were not



561 available from every plot, so to ensure consistent treatment of plots height-diameter models were  
562 constructed for each biogeographic region. We fitted three parameter asymptotic models (47) of the  
563 form

$$564 \quad H = a(1 - \exp(-bD^c)), \quad [3]$$

565 where  $a$ ,  $b$  and  $c$  are estimated parameters ('Weibull' models, 48). We fitted these models either  
566 treating each observation equally or with case weights proportional to each trees' basal area. These  
567 weights give more importance to large trees during model fitting. We selected the best fitting of these  
568 models, determining this as the model that minimised prediction error of stand biomass when  
569 calculated with estimated heights or observed heights (46). Weibull models were implemented using  
570 the nls function in R with default settings. Starting values of  $a = 25$ ,  $b = 0.05$  and  $c = 0.7$  were chosen  
571 following trial and error as they led to regular model convergence. Where models did not converge  
572 this was usually because the height-diameter relationship did not reach an asymptote, so in these cases  
573 we used the log-log model  $\ln(H) = a + b(\ln(D))$  to estimate height, where  $b$  gives the scaling exponent  
574 of a power law relationship between height and diameter. We checked if models gave unrealistic  
575 predictions by applying models to predict the height of all trees in the biogeographic region, and  
576 excluded models that predicted any tree height 10 % higher than the tallest tree we recorded in that  
577 continent.

578

### 579 Estimating above-ground woody production

580 We estimated AGWP following Talbot et al. (37). AGWP is comprised of four components, (1) the  
581 sum of growth of surviving trees, (2) the sum of AGB of new recruits, (3) the sum of unobserved  
582 growth of trees that died during a census interval and (4) the sum of growth of unobserved recruits  
583 that entered then died during a census interval. Accounting for the latter two components is necessary  
584 to avoid census-interval length effects, as more AGWP in these components will be missed due to the  
585 greater mortality of trees that accumulates over longer census intervals.

586 Components 3 and 4 can be estimated using two quantities that can be calculated from observed stem-  
 587 dynamics in each plot; per-area annual recruitment ( $R_a$ ) and per-capita annual mortality ( $m_a$ ). Per-  
 588 capita mortality is calculated from the ratio of surviving stems to initial stems, using equation 5 in  
 589 Kohyama et al. (49). Per-area annual recruitment is calculated using estimated mortality rates and the  
 590 observed change in the number of stems over a census interval, using equation 11 of Kohyama et al.  
 591 (49).

592 To estimate the unobserved growth of stems that died during a census interval, we first use plot-level  
 593 per-capita mortality rates ( $m_a$ ) to estimate how many trees are expected to have died in each year of  
 594 the census interval, and from that calculate the mean number of years that trees that died during the  
 595 census interval would have lived before death. The diameter of tree at death ( $D_{\text{death}}$ ) can then be  
 596 estimated as

$$597 \quad D_{\text{death}} = D_{\text{start}} \times G \times Y_{\text{mean}} \quad [4]$$

598 where  $D_{\text{start}}$  is the diameter at the start of the census interval,  $G$  is the plot-level median growth rate of  
 599 the size class the tree was in at the start of the census interval (size classes are defined as  $D < 200$  mm,  
 600  $400 \text{ mm} > D \geq 200$  mm, and  $D \geq 400$  mm) and  $Y_{\text{mean}}$  is the mean number of years trees survived in  
 601 the census interval before dying. The diameter at death is then converted to AGB at death using  
 602 allometric equations (equation 1, except for ferns and monocots where equation 2 is used), and the  
 603 unobserved growth is calculated as the difference between AGB at death and AGB at the start of the  
 604 census.

605 To estimate the growth of recruits that were not observed because they died during the census  
 606 interval, we first need to estimate the number of unobserved recruits. This can be estimated from per-  
 607 area annual recruitment ( $R_a$ ) and per-capita annual mortality ( $m_a$ ):  $R_a$  gives the number of stems per ha  
 608 that recruit in a given year, and the probability of each recruit surviving until the next census ( $P_{\text{surv}}$ ) is  
 609  $P_{\text{surv}} = (1 - m_a)^T$ , where  $T$  is the number of years remaining in the census interval. The number of  
 610 recruits in a given year that survive to the next census is  $R_a - P_{\text{surv}}R_a$ . Summing this for each year in a  
 611 census interval gives the total number of unobserved recruits in that census interval. We then need to

612 estimate how long each recruit was alive for. From  $m_a$  we can calculate the number of recruits in a  
613 given year that died in each subsequent year, and from this calculate the mean life-span of recruits in a  
614 given year that died before the next census. The average life-span of unobserved recruits ( $Y_{mean-rec}$ ) is  
615 the weighted mean of each cohort's lifespan, weighted by the number of unobserved recruits in each  
616 year. Diameter at death is given in mm by

$$617 \quad D_{death} = 100 + (G \times Y_{mean-rec}) \quad [5]$$

618 where  $G$  is the plot-level median growth rate of the smallest size class (i.e.  $D < 200$  mm).

619 Aboveground biomass of recruits at the time of death is estimated using equation 1. These corrections  
620 for unobserved growth have a marginal impact on AGWP calculations, collectively accounting on  
621 average for just 2.3 % of estimated plot-level AGWP.

622 AGB was calculated for each census, and AGWP was calculated for each census interval, and the  
623 time-weighted mean of each was taken to give one value per plot. We used a time-weighted mean to  
624 give greater importance to AGB estimates separated by longer census-intervals, as these will be more  
625 independent. Estimates of AGB and AGWP were converted to carbon stocks and carbon gains by  
626 multiplying by 0.456 (50). Carbon residence time was then estimated as carbon stocks /carbon gains,  
627 and represents the length of time carbon resides in living biomass before being passed to the litter and  
628 necromass pools (51). Calculations to estimate AGB and AGWP were performed using the R package  
629 BiomasaFP (52).

630

### 631 Obtaining environmental data

632 Most climate data were obtained from climate data from Worldclim2 (31) as it provides the highest  
633 resolution (~ 1 km) pantropical climate data, although we note that some regions, such as central  
634 Africa, have limited station data. We extracted monthly data for the following variables: mean daily  
635 minimum temperature, mean daily maximum temperature, precipitation, solar radiation and wind  
636 speed, In addition to calculating the standard series of 19 bioclimatic variables, using the dismo R  
637 package (53), we calculated 1) mean daily maximum temperature,  $BIO1 + BIO2/2$ , 2) mean daily

638 minimum temperature, BIO1 – BIO2/2, 3) maximum cumulative water deficit as the minimum across  
639 the year of monthly cumulative water deficit  $W$ ,

$$640 \quad W_i = W_{i-1} - \min(0, P_i - 100), \quad [6]$$

641 where  $P$  is monthly precipitation in mm, and 100 represents measured evapotranspiration. This  
642 calculation was run for a year from the wettest month in the year, starting at a water deficit of zero, 4)  
643 the number of months where monthly cumulative water deficit was negative, 5) the number of months  
644 where monthly precipitation was below 100 mm (i.e. less than evapotranspiration), 6) mean annual  
645 solar radiation, 7) mean annual wind speed, and 8) vapour pressure deficit ( $VPD = SVP - \text{vapour}$   
646  $\text{pressure}$ , where saturated vapour pressure,  $SVP, = 0.611 \times e^{(17.502 \text{ temperature}) / (\text{temperature} + 240.97)}$ ). We also  
647 obtained data on cloud frequency at ~1 km resolution from Wilson & Jetz (54), who processed twice-  
648 daily MODIS satellite images. Temperature values were adjusted for differences in altitude between  
649 the plot and the 1 km grid cell used for Worldclim interpolation, as these can differ in topographically  
650 diverse regions, using lapse rates, so that  $T_{plot} = T_{worldclim} + 0.005 \times (A_{worldclim} - A_{plot})$ , where  $T$  is  
651 temperature ( $^{\circ}\text{C}$ ) and  $A$  is altitude (m). Temperature values were also corrected for systematic  
652 warming trends. To do this, the mean annual temperature in each grid-cell in each year was extracted  
653 from the CRU TS 3.24 dataset (55), and robust linear regression used to estimate grid-cell specific  
654 warming rates. These were used to adjust Worldclim2 temperature values for the difference between  
655 the midpoint of plot monitoring and the midpoint of the Worldclim2 climatology.

656 Data on soil texture and chemistry was obtained at 1 km resolution from the SoilGrids dataset (56),  
657 with this resolution selected to match the resolution of the climate data. From this we extracted CEC,  
658 representing soil fertility, and percentage clay, representing soil texture. For each soil variable we  
659 calculated the depth-weighted average for 0 – 30 cm.

## 660 Statistical analysis

661 We used linear models to relate carbon, carbon gains and carbon residence time to environmental  
662 explanatory variables. The role of different explanatory variables was assessed using multi-model  
663 inference.

664 Response variables were positively skewed and had positive mean-variance relationships, so were  
665 log-transformed to meet the assumption of normality and reduce heterogeneity in variances. The log-  
666 normal nature of forest carbon stocks and dynamics means that there is greater potential for variation  
667 when forests are large, which could be due to the non-linear scaling of tree biomass and tree basal  
668 area.

669 We selected explanatory variables to represent hypothesised ways in which climate could affect  
670 carbon stocks (Table S1). We assessed collinearity within this set of explanatory variables using  
671 variance inflation factors (VIF) and pairwise correlations. Because of collinearity, we had to exclude  
672 VPD, total precipitation, use only one of MCWD and precipitation in the driest quarter, and could  
673 include both minimum and maximum temperature but not mean annual temperature. We used  
674 precipitation in the driest quarter rather than MCWD as the latter is zero truncated and so is less  
675 amenable to regression analysis. After removing these variables all pairwise correlations (including  
676 with soil explanatory variables) were weak enough not to cause problems through collinearity ( $r < 0.6$   
677 and  $VIF < 3$ ).

678 To account for variation other than in climate we also included soil variables relating to texture (%  
679 clay) and fertility (CEC), and included continent specific intercepts to account for biogeographic  
680 variation in carbon. To account for unmeasured environmental gradients (e.g. soil variation not  
681 captured by the SoilGrids variables), we used Moran's eigenvector maps as explanatory variables,  
682 selecting eigenvectors that corresponded to positive spatial autocorrelation in the distance matrix (57).  
683 These variables act as a proxy for unmeasured spatial gradients by capturing positive spatial  
684 associations between plots.

685 Plots differed in their area and the length of time they were monitored for. This is likely to affect the  
686 variance of carbon stocks, carbon gains and carbon residence time, as smaller plots or plots only  
687 monitored for short periods are more likely to be sensitive to the mortality of a few large trees. To  
688 account for this, we used case weights relating to plot area and monitoring period. Following Lewis et  
689 al. (58), we selected weights by relating residuals from our linear models to plot area and to plot  
690 monitoring period, and subsequently assessing which root transformation of plot area/ monitoring

691 period removed the pattern in the residuals when used as a weight. Selected weights were: carbon  
692 stocks, Area<sup>1/3</sup>; carbon gains, Monitoring length<sup>1/7</sup>; carbon residence time, Area<sup>1/9</sup> + Monitoring  
693 length<sup>1/12</sup> -1.

694 We fitted all subsets of the general linear model with explanatory variables described above, forcing  
695 spatial eigenvectors into all models. We then averaged the subset of models where  $\Delta AIC < 4$ , using  
696 full averaging so variables that do not appear in the model get the value of zero for their coefficients.  
697 This means that model averaged coefficients of terms with limited support exhibit shrinkage towards  
698 zero. Multi-model inference was performed using the MuMIn R package (59).

699 We assessed whether the two climate variables found to have important additive effects on carbon  
700 stocks in this analysis (mean daily maximum temperature in the warmest month and precipitation in  
701 the driest quarter) interacted with each other by adding an interaction term between these variables to  
702 the full generalised linear model of carbon stocks as a function of other climate and soil variables,  
703 continent and spatial eigenvectors. We compared these two models using AIC. We repeated this with  
704 carbon gains and carbon residence time as response variables.

705 To assess whether the temperature carbon relationship was non-linear we used breakpoint regression  
706 implemented in the segmented R package (60). This estimates a breakpoint in the explanatory variable  
707 at which the slope of the relationship with the response variable changes. We estimated the breakpoint  
708 for the mean daily maximum temperature in the warmest month variable in the full model with a  
709 temperature-precipitation interaction described above. We assessed the support for the breakpoint by  
710 comparing the AIC of the model with a breakpoint with the AIC of a model with a linear relationship.  
711 We repeated this with carbon gains and carbon residence time as response variables.

712 We also analysed spatial variation in carbon stocks as a function of the above climate and soil  
713 variables and spatial eigenvectors using Random Forest decision tree algorithms (22) implemented  
714 using the randomForest R package (61). We assessed variable importance by calculating the average  
715 increase in node purity across all decision trees (measured by residual sum of squares) when using the  
716 variable to split the data. We assessed modelled relationships between response and explanatory

717 variables using partial plots, which show predicted change in the response variable, averaged across  
718 trees, when changing the explanatory variable and holding all other variables constant.

719 To compliment this analysis based on relationships expected *a priori*, we also performed an  
720 exploratory analysis to assess whether other climate variables excluded from the full general linear  
721 models had an effect on carbon. To do this, we fitted linear models to assess the bivariate relationship  
722 of carbon with each climate variable, with continent also included as an explanatory variable to  
723 account for biogeographic variation in forest characteristics.

724

#### 725 Validation with independent single-census plot dataset

726 We assessed whether the relationships with environmental variables identified in the analyses of  
727 multi-census plot data described above held when applied to an additional dataset of 223 single-  
728 census plots. As the single-census data were not used in any of the analyses above they did not  
729 influence modelling decisions, so provide an independent test of the relationships identified with the  
730 multi-census plot analysis.

731 Single-census plots were extracted from the ForestPlots.net database (39, 40) using the same plot-  
732 selection criteria as for the multi-census plots, except that censuses during or following the 2015-16  
733 strong El Niño were included in the single-census plot dataset as we expected that carbon stocks,  
734 unlike gains, would still remain close to their long-term mean.

735 We fitted a general linear model with the five climate explanatory variables, soil fertility and texture,  
736 continent and spatial eigenvector, and model averaging of all subsets of this model as described for  
737 the multi-census plots. We performed this analysis using just the single-census plots and a combined  
738 dataset of single and multi-census plots.

739

#### 740 Scaling results to the biome

741 We applied the relationship between carbon stocks and mean daily maximum temperature in the  
742 warmest month identified by the breakpoint regression to estimate the total change in carbon stock  
743 due to temperature effects alone for different scenarios of temperature increase. We delimited the  
744 biome extent using the WWF tropical and subtropical moist broadleaved forest biome (62), restricted  
745 to tropical latitudes, and further refined it by excluding grid-cells with  $< 50 \text{ Mg C ha}^{-1}$  using data from  
746 (30), as these are unlikely to be forest. Calculations were conducted at 10-minute resolution. For each  
747 grid-cell we predicted the percentage change in carbon for a given temperature increase from our  
748 statistical model, holding all other variables constant. We then used a reference carbon stock map (30)  
749 to convert percentage change to change in carbon stocks per hectare (in  $\text{Mg ha}^{-1}$ ). To calculate change  
750 in carbon stocks for the whole grid-cell, we multiplied change per hectare by the area of the grid-cell  
751 in hectares, and then adjusted this by the proportion of the grid-cell that was forested by multiplying  
752 by 2014 forest cover (63). Total change for the biome (in Pg) was calculated by summing these grid-  
753 cell level values. Uncertainty due to our statistical model was assessed by generating multiple  
754 predictions by resampling model parameters (breakpoint threshold, slope below breakpoint, slope  
755 above breakpoint), and extracting quantiles from the resultant distribution of predicted change values.  
756 Aboveground biomass carbon values were scaled to include root biomass based on a root to shoot  
757 ratio of 0.19 in tropical evergreen forests (64).

758 The Avitabile et al (30) aboveground biomass map was chosen to provide reference carbon stocks.  
759 While other maps have previously been produced by Saatchi et al. (65) and Baccini et al. (66) we  
760 selected the Avitabile map because it synthesises the earlier maps (see Mitchard et al. (67) for  
761 discussion of substantial differences between these maps) and is anchored by more field data.  
762 Importantly, the Avitabile map reproduces spatial patterns in aboveground biomass that have been  
763 described from field data but are absent in the Saatchi or Baccini maps, including the much higher  
764 biomass density of north-east Amazonian forests due to tall trees and very high wood density (68).  
765 Nevertheless, we also investigated the consequences of using the Saatchi or Baccini maps for our  
766 estimates of biomewide thermal sensitivity and spatial patterns of change in carbon stocks (Fig S15).



767 We investigated three temperature change scenarios. Firstly, we applied a 1°C increase to all  
768 locations. Secondly, we assessed the consequence of a 1.5°C increase in global temperature from pre-  
769 industrial levels for the equilibrium temperature response of tropical forest carbon. Finally, we  
770 assessed the consequence of a 2°C increase in global temperature from pre-industrial levels. For the  
771 latter two we obtained data from CMIP5 climate models, using downscaled future climate projections  
772 based on the Worldclim climatology (69). As downscaling was performed using Worldclim version  
773 1.4 (70) and our statistical models use Worldclim version 2, we calculated the warming anomaly in  
774 each grid-cell from the current Worldclim version 1.4 conditions, and applied this to the Worldclim 2  
775 data to obtain future temperature. RCP scenarios and time-points were chosen to give global  
776 temperature increases that best match 1.5°C and 2°C above pre-industrial. For 1.5°C we used RCP 2.6  
777 averaged for 2040-2060 (median temperature increase across models = 1.5°C, (71)). For 2°C, we used  
778 RCP 2.6 averaged for 2040-2060 (median temperature increase models = 1.9°C (71)). Note that  
779 predicted increases in maximum temperatures were often considerably greater than the global  
780 increase, especially in South America. For both scenarios we used the median predicted temperature  
781 change for each grid-cell from an ensemble of 15 models (BCC-CSM1-1, CCSM4, CNRM-CM5,  
782 GFDL-CM3, GFDL-ESM2G, GISS-E2-R, HadGEM2-AO, HadGEM-ES, IPSL-CM5A-LR, MIROC-  
783 ESM-CHEM, MIROC-ESM, MIROC5, MPI-ESM-LR, MRI-CGCM3, NorESM1-M).

784 We assessed the potential for long-term carbon dioxide growth stimulation to offset these long-term  
785 temperature effects. We used CO<sub>2</sub> concentrations from the RCP scenarios and time-points described  
786 above, which approximate the long-term concentrations if the climate stabilised at the new  
787 temperatures (72). Thus the 1.5°C and 2°C scenarios were associated with CO<sub>2</sub> concentrations of 443  
788 ppm and 487 ppm respectively (73). We cannot assess the effect of CO<sub>2</sub> on biomass from our spatial  
789 dataset, so instead used independent estimates of CO<sub>2</sub> effects from other sources. Firstly, we obtained  
790 CO<sub>2</sub> only effects on net primary production (NPP) extracted from an ensemble of CMIP5 earth system  
791 models by (74). This gives the proportional change in NPP for evergreen forests (note that this also  
792 includes boreal forests) over 1980-2010, standardised to a 100 ppm increase in CO<sub>2</sub> concentration. To  
793 propagate this through to changes in AGB under future CO<sub>2</sub> conditions we first estimated the

794 logarithmic dependency of NPP on CO<sub>2</sub> (75) by substituting values of NPP and CO<sub>2</sub> at time zero and  $t$   
 795 (from (74)) into the equation,

$$796 \quad NPP_t = NPP_0 \left[ 1 + \beta \ln \left( \frac{[CO_2]_t}{[CO_2]_0} \right) \right] \quad [7]$$

797 This equation can be used to compute NPP annually given an initial NPP estimate and a time series of  
 798 atmospheric CO<sub>2</sub> concentrations (from a combination of the observed record from pre-industrial and  
 799 the RCP 4.5 scenario, modified so that it stabilises at 487 or 443 ppm depending on warming  
 800 scenario). Initial pre-industrial NPP was back-calculated from present-day values using Equation 7,  
 801 with 13.3 Mg C ha<sup>-1</sup> yr<sup>-1</sup> (mean of nine Amazon plots where NPP has been measured, from (76)) used  
 802 for present-day NPP. To propagate NPP into change in woody biomass (following (51)) we used the  
 803 equation

$$804 \quad \frac{dM_{wood}}{dt} = \alpha_{wood} N_P - \frac{M_{wood}}{\tau_{wood}} \quad [8]$$

805 where  $M_{wood}$  is woody biomass,  $N_p$  is NPP,  $\alpha_{wood}$  is the allocation of NPP to wood (taken as 0.33, the  
 806 mean value across nine plots from (76)) and  $\tau_{wood}$  is the residence time of woody biomass, taken as  
 807 59.1 years (the median value across plots used in this study). This model (equations 7 and 8) was run  
 808 from pre-industrial to 2500, enabling us to see the equilibrium effect of increased CO<sub>2</sub> concentrations  
 809 on biomass, assuming temporally invariant allocation and residence time. We calculated the  
 810 proportional change in biomass from 2000 to 2500, and applied this to the reference carbon stock map  
 811 to obtain predicted equilibrium change in aboveground biomass due to CO<sub>2</sub> effects.

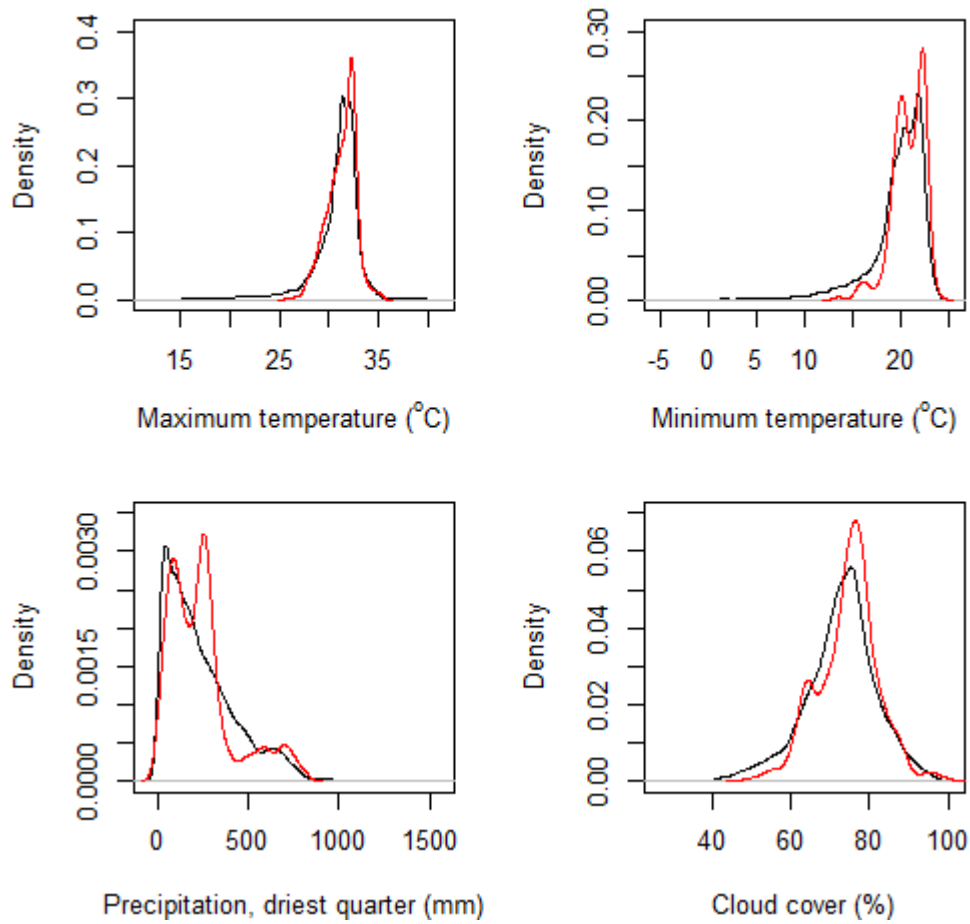
812 The effects of CO<sub>2</sub> in earth system models have been reported to be larger than those deduced from  
 813 satellite data or CO<sub>2</sub> enrichment experiments (74), so we also ran the above model using changes in  
 814 NPP reported from a synthesis of free-air CO<sub>2</sub> enrichment experiments conducted in forests (74).  
 815 Finally, we looked at the impact of using CO<sub>2</sub> effects derived from a recent large meta-analysis of  
 816 CO<sub>2</sub> enrichment experiments (77), which reported a 12.5 % increase in biomass of tropical trees for a  
 817 250 ppm increase in CO<sub>2</sub> concentration. As this relationship was reported to be linear (77) we used  
 818 linear interpolation to estimate the change in biomass under CO<sub>2</sub> concentrations associated with each

819 warming scenario (i.e. 443 and 487 ppm). To estimate long-term changes in biomass accounting for  
820 both temperature and carbon dioxide, we first applied the CO<sub>2</sub> relationship to estimate the change in  
821 biomass due to carbon dioxide growth stimulation, and then assessed the effects of warmer  
822 temperatures from this revised baseline. Our approach allows a simple assessment of CO<sub>2</sub> effects  
823 exploring a range of different effect strengths. Real-world responses will likely be more complex,  
824 with, for example, nutrient limitation potentially affecting the extent to which growth is stimulated by  
825 CO<sub>2</sub> (77).

826

827

828



829

830

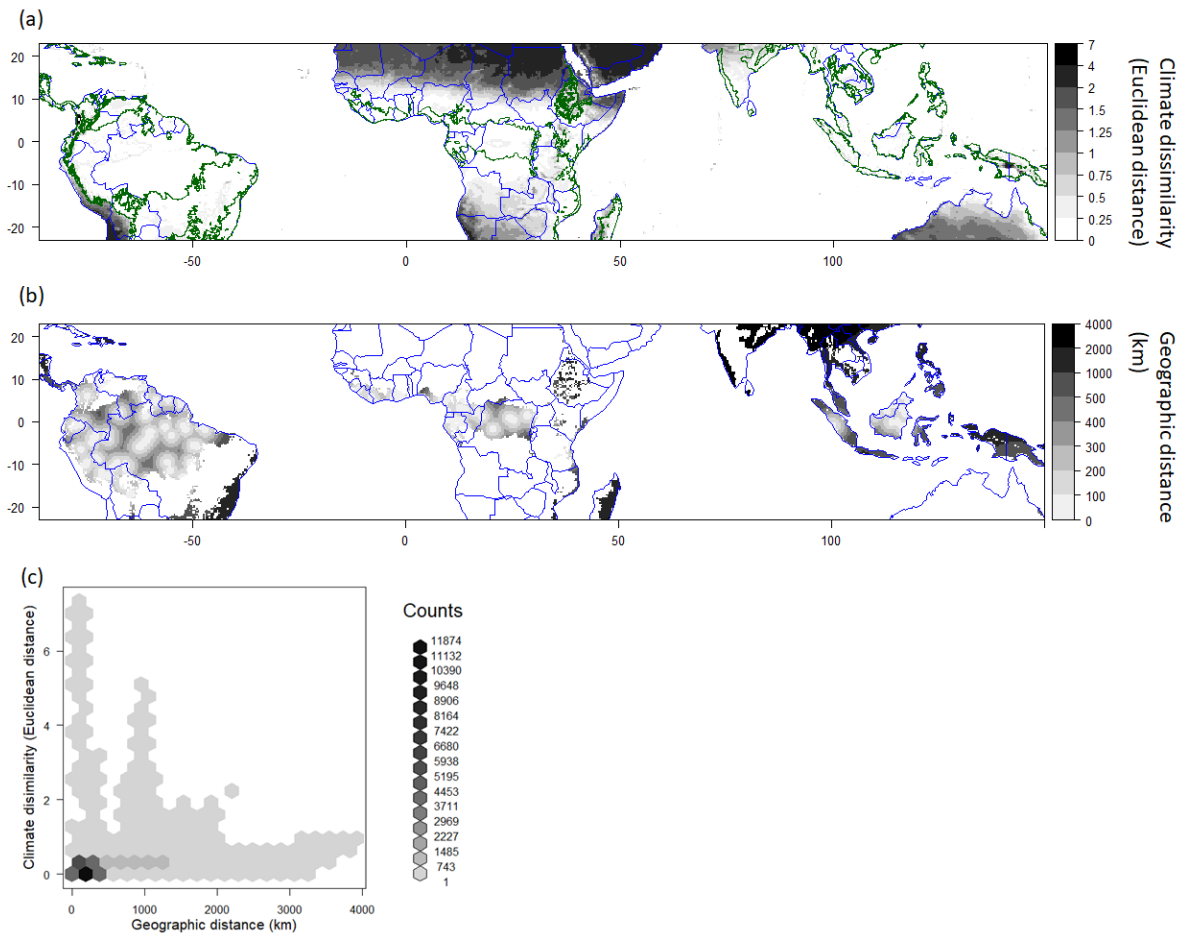
831

832

833

**Figure S1.** Climate space represented by our plot network. Red lines show the probability density function of each variable in our multi-census plot network. Black lines show the probability density across 10 minute grid-cells in the biome, restricted to areas with forest cover in GLC 2000 (78).

834



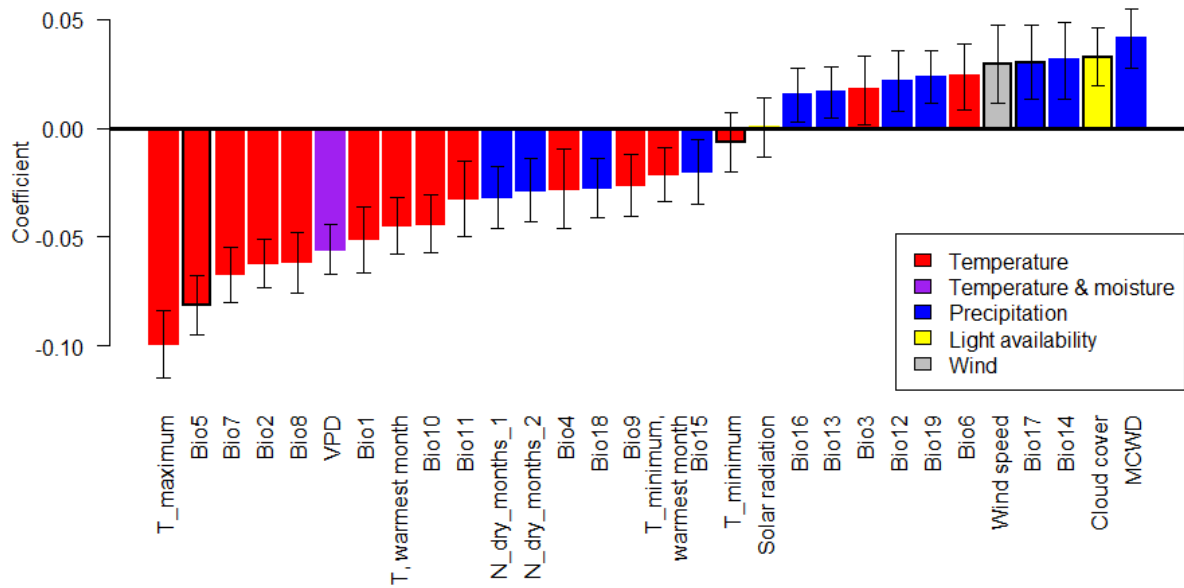
835

836 **Figure S2.** Ability of our plot network to represent the climate conditions found in the moist tropical  
 837 forest biome. (a) Minimum climate dissimilarity (measured as Euclidean distance on climate variables  
 838 scaled by their standard deviation) between 10 minute grid cells and the multi-census plot network.  
 839 Climate variables used are the same as in Fig. 2. Green lines indicate the extent of the biome. (b)  
 840 Geographic distance (km) between grid cells and the multi-census plot network. (c) Relationship  
 841 between climatic and geographic distance of 10 minute grid cells across the tropical forest biome to  
 842 our plot network. The lack of relationship between climate dissimilarity and geographical distance,  
 843 alongside the mostly low climatic dissimilarities, shows that our sampling is sufficient to capture the  
 844 environmental space of the biome and that we can reasonably extrapolate to geographically distant  
 845 areas from our plots, which are in any case largely deforested already and hence contribute very little  
 846 to our projected biome-wide carbon response to climate change. (These tropical moist forest areas that  
 847 are poorly sampled and largely lost include the Atlantic Forests in Brazil, Andean Forests in western

Supporting information for Sullivan et al.

848 South America, eastern Caribbean, Madagascar, and much of tropical South Asia, south China,  
849 continental Southeast Asia, Philippines, Sumatra and Java).

850



851

852 **Figure S3.** Relationships between individual climate variables and tropical forest aboveground carbon

853 stocks. Standardised coefficients are from models with the climate variable and continent as

854 explanatory variables and show change in  $\ln(\text{carbon})$  for a standard deviation change in the

855 explanatory variable. Error bars show standard errors. Variables used in the main analysis have black

856 outlines. Full variable names are: T\_maximum – mean daily maximum temperature, Bio5 – mean

857 daily maximum temperature in the warmest month, Bio7 – annual temperature range, Bio2 – mean

858 diurnal temperature range, Bio8 – mean temperature in the wettest quarter, VPD – vapour pressure

859 deficit, Bio1 – mean annual temperature, Bio10 – mean temperature in the warmest quarter, Bio11 –

860 mean temperature in the coldest quarter, N\_dry\_months\_1 – number of months with negative

861 cumulative water deficit, N\_dry\_months\_2 – number of months where precipitation is less than

862 evapotranspiration, Bio4 – temperature seasonality, Bio18 – precipitation in the warmest quarter, Bio9

863 – mean temperature in the driest quarter, T\_minimum warmest month – mean daily minimum

864 temperature in the warmest month, Bio15 – precipitation seasonality, T\_minimum – mean daily

865 minimum temperature, Bio16 – precipitation in the wettest quarter, Bio13 – precipitation in the

866 wettest month, Bio3 – isothermality, Bio12 – annual precipitation, Bio19 – precipitation in the coldest

867 quarter, Bio6 – mean daily minimum temperature in the coldest month, Wind speed – mean daily

Supporting information for Sullivan et al.

868 wind speed, Bio17 – precipitation in the driest quarter, Bio14 – precipitation in the driest month,  
869 Cloud cover – proportion of MODIS passes with cloud present, MCWD – maximum cumulative  
870 water deficit (note this is negative when water deficit is high, so a positive relationship with MCWD  
871 indicates higher carbon when water deficits are less).

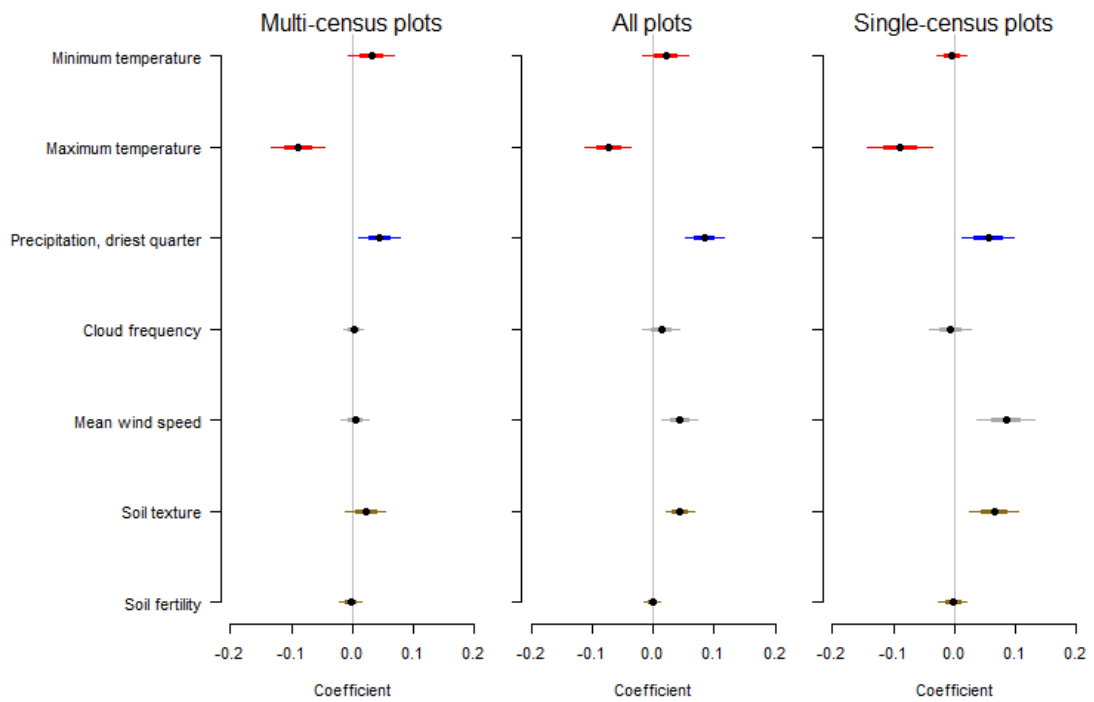
872

873



874

875



876

877 **Figure S4.** Validation of tropical forest carbon stock sensitivity model against an independent dataset

878 of 223 single-census plots from our networks measured with the same protocols. Model-averaged

879 shrinkage adjusted coefficients from multiple regression models of biomass carbon stocks as a

880 function of climate, soil, biogeography and spatial eigenvectors. Models were either fitted to the

881 multi-census plot dataset (as in Fig. 2), to the single-census plot dataset, or to the combined dataset.

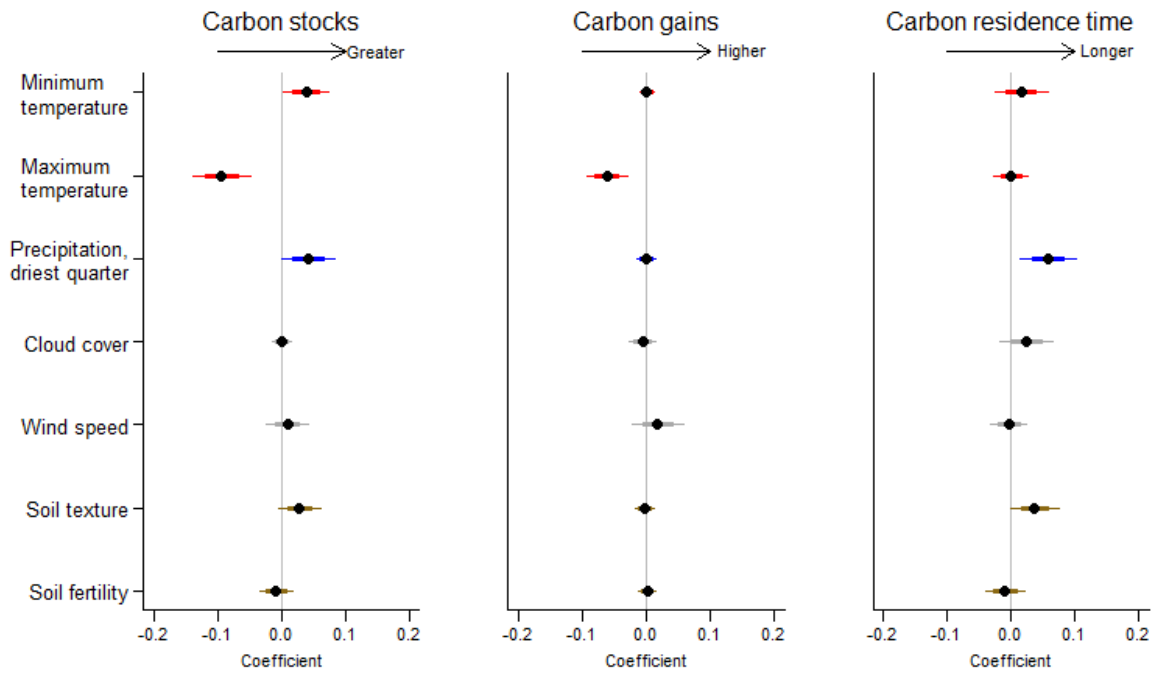
882 This analysis shows that the relationships identified to be most important in the main multi-census

883 plot analysis (i.e. the negative relationship between carbon stocks and maximum temperature and

884 positive relationship with precipitation in the driest quarter) are also found in an independent dataset,

885 which was not used for preliminary analysis so did not influence the choice of explanatory variables.

886



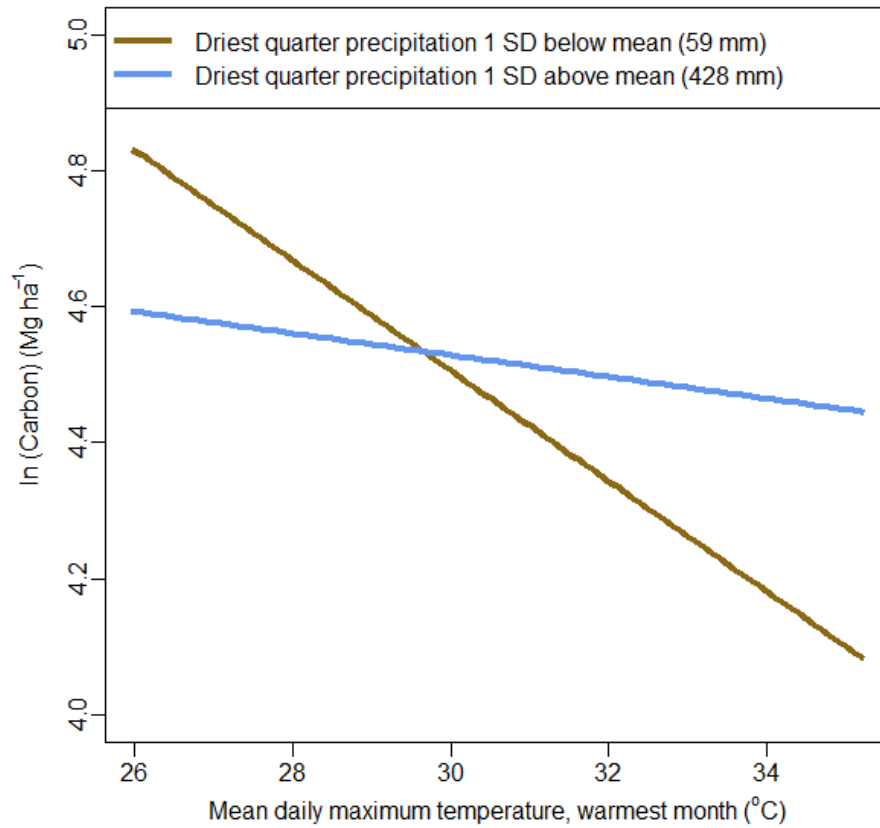
887

888 **Figure S5.** As Figure 2, but with aboveground biomass estimated using the Chave et al. 2005 (79)  
889 moist forest allometric equation, which does not include a height term and is instead based on a third-  
890 order polynomial relationship between diameter and aboveground biomass. This indicates that our  
891 results are robust to using an alternative allometry to estimate aboveground biomass.

892

893

894

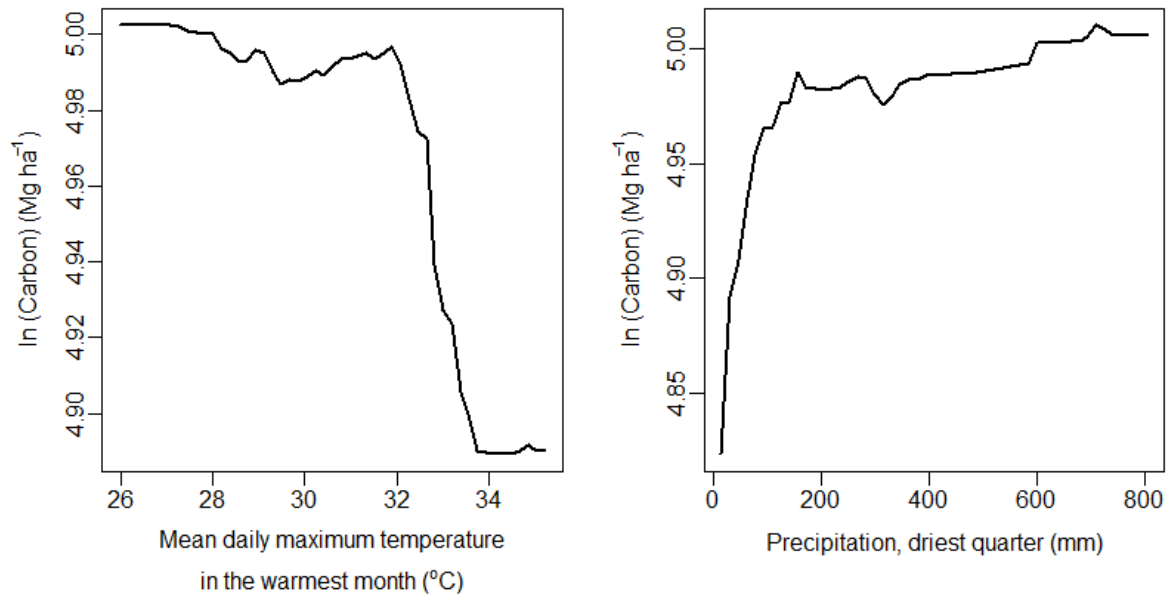


895

896 **Figure S6.** Interaction between mean daily maximum temperature in the warmest month and  
897 precipitation in the driest quarter in determining aboveground tropical forest carbon stocks. Modelled  
898 relationships with temperature are shown holding precipitation either one standard deviation above or  
899 below the mean. Note that the temperature-carbon relationship is steeper when precipitation is low.

900

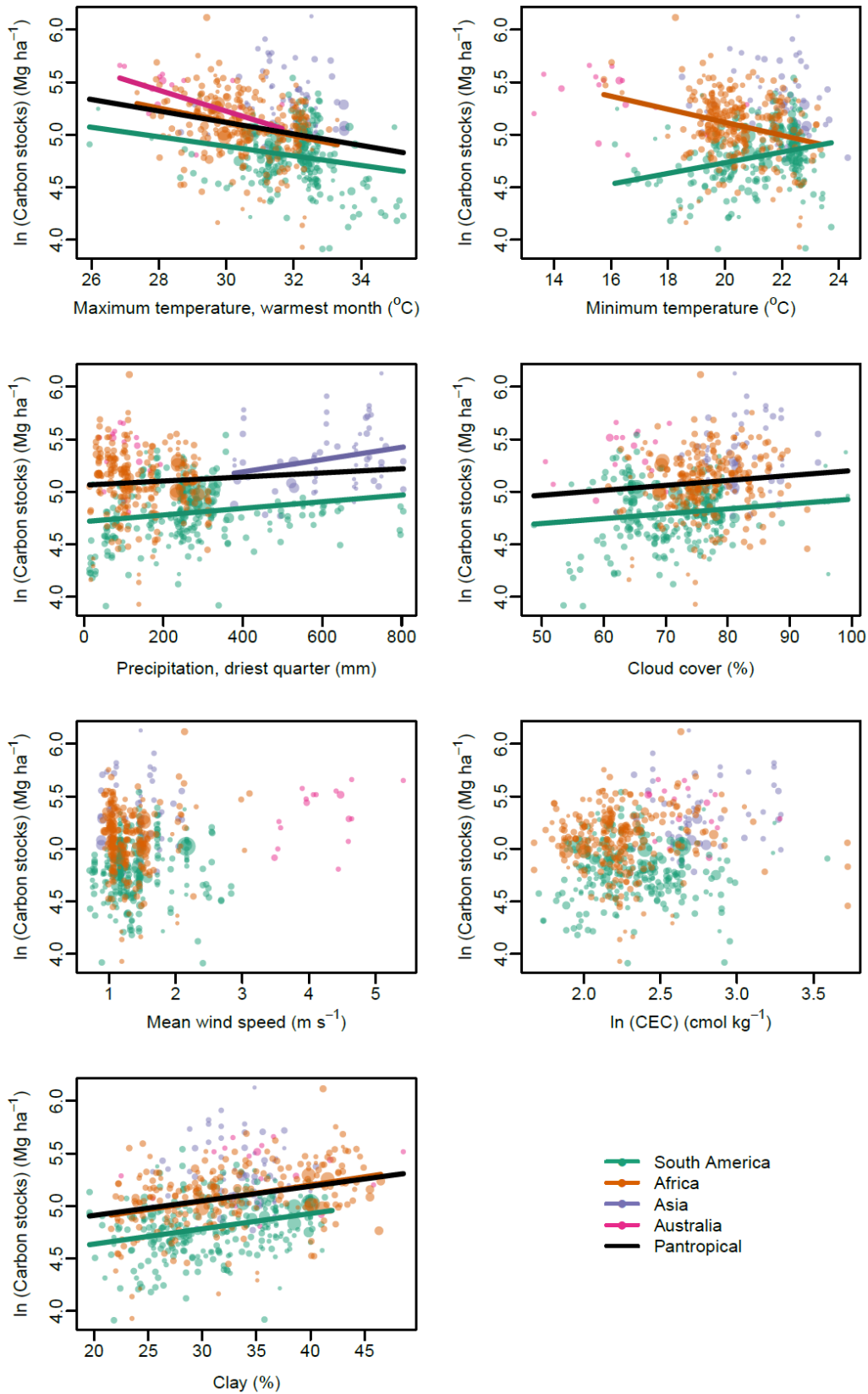
901



902

903 **Figure S7.** Partial relationships between tropical forest carbon stocks and the two climate variables  
904 identified to be most important by the random forest decision tree algorithm. Partial plots show  
905 predicted values of carbon stocks averaged across an ensemble of decision tree models when  
906 changing the explanatory variable of interest and holding other variables constant. The importance of  
907 variables in random forest analysis is assessed by calculating the average increase in node purity  
908 across all decision trees (measured by residual sum of squares) when using the variable to split the  
909 data. Higher values indicate greater importance. Maximum temperature increased node purity by 4.8  
910 and precipitation by 4.7. For all other climate variables increases in node purity were < 3.5.

911



912

913 **Figure S8.** Relationships between aboveground tropical forest carbon stocks and environmental

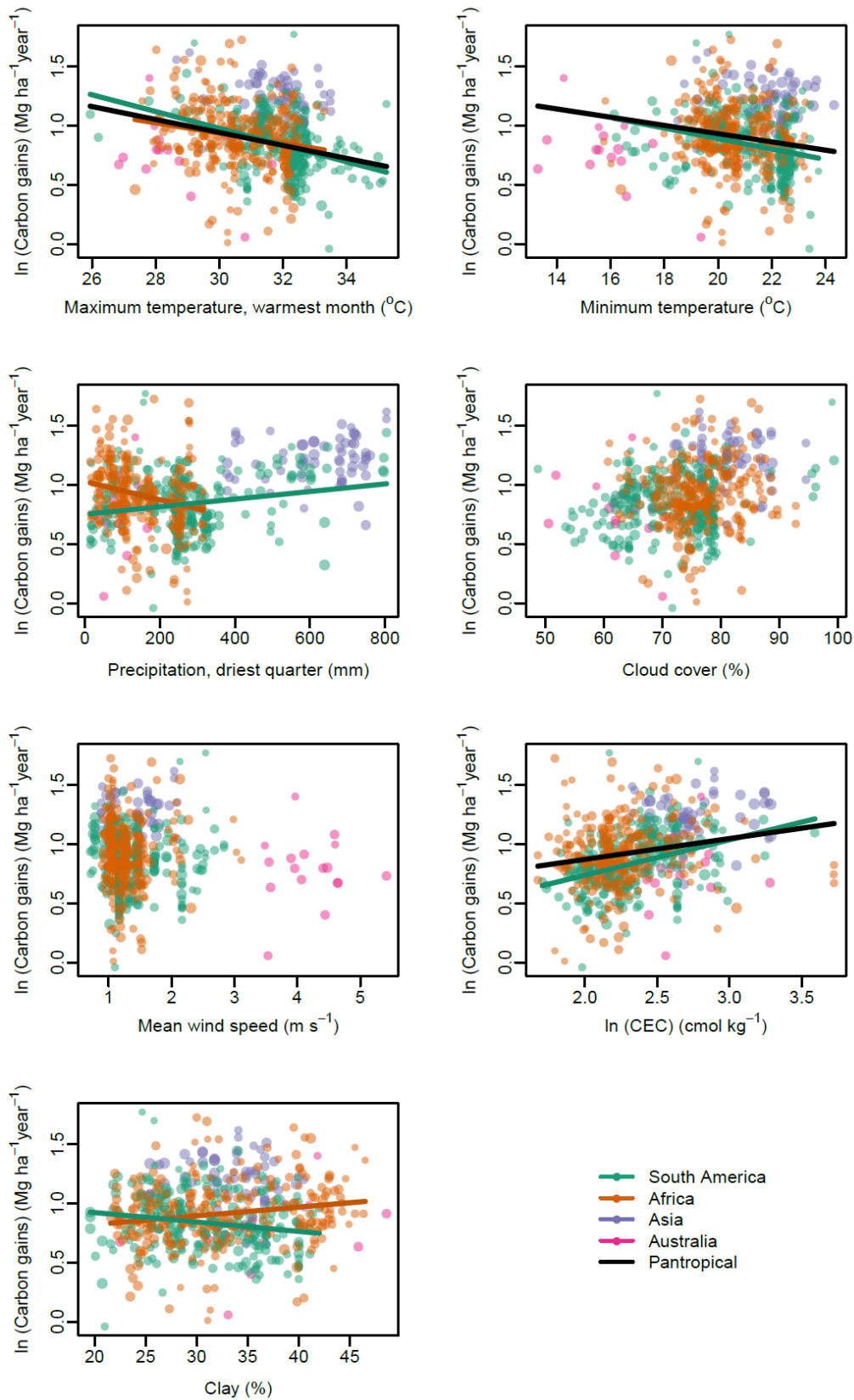
914 predictors. Symbols and colours as in Fig. 3. Coloured lines show bivariate relationships in each

Supporting information for Sullivan et al.

915 continent, and black lines show pan-tropical relationships also accounting for the effect of continent.

916 Lines are only plotted where statistically significant.

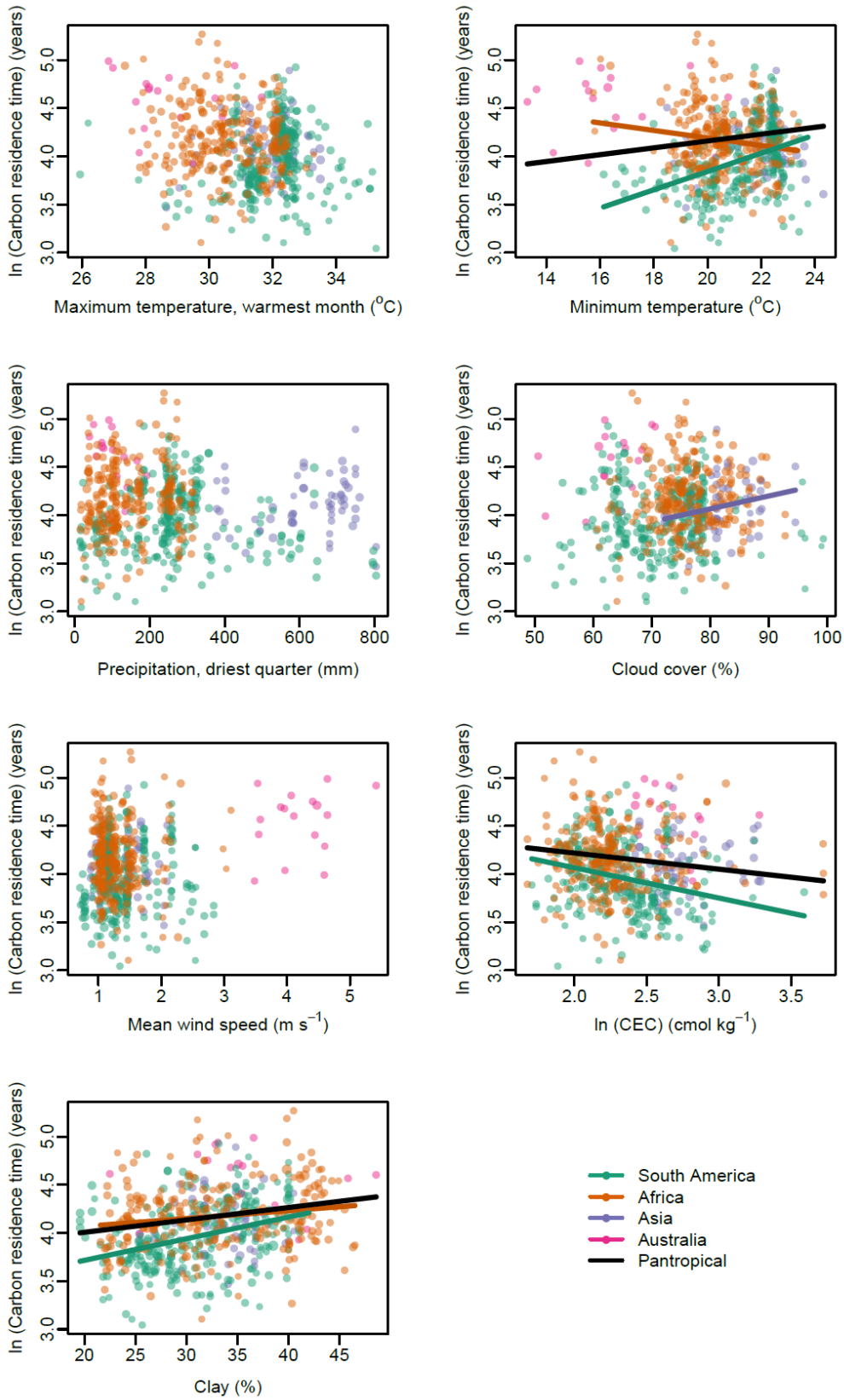
917



918

919

920 **Figure S9.** As Fig. S8, but showing relationships with carbon gains.

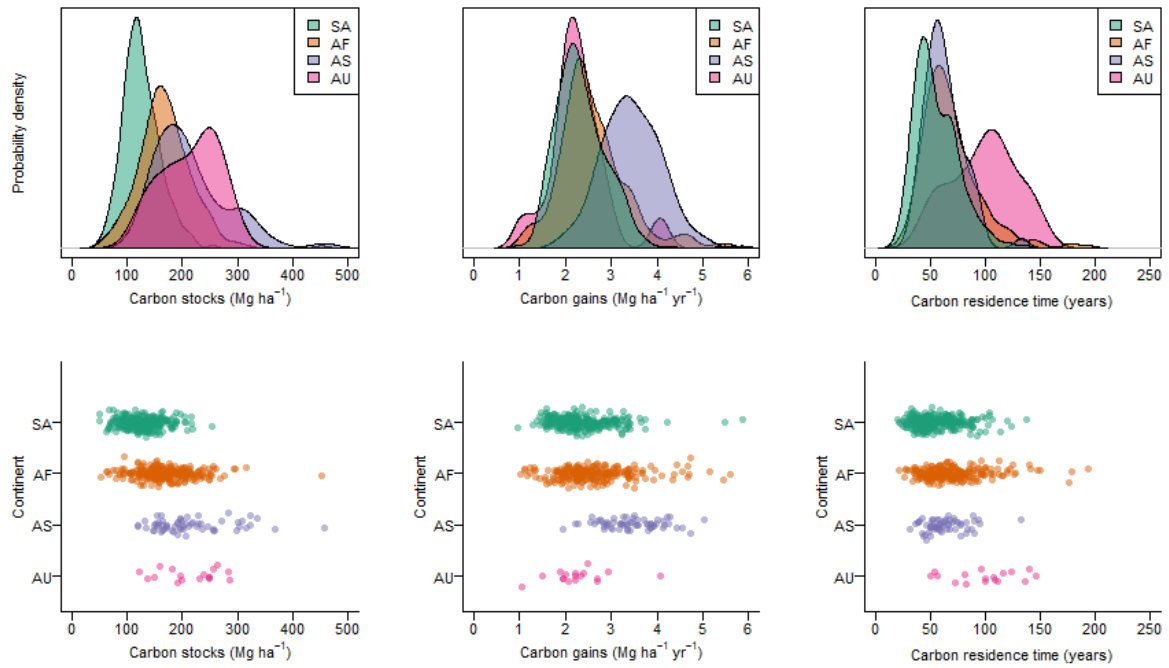


921

922 **Figure S10.** As Fig. S8, but showing relationships with carbon residence time.

923





924

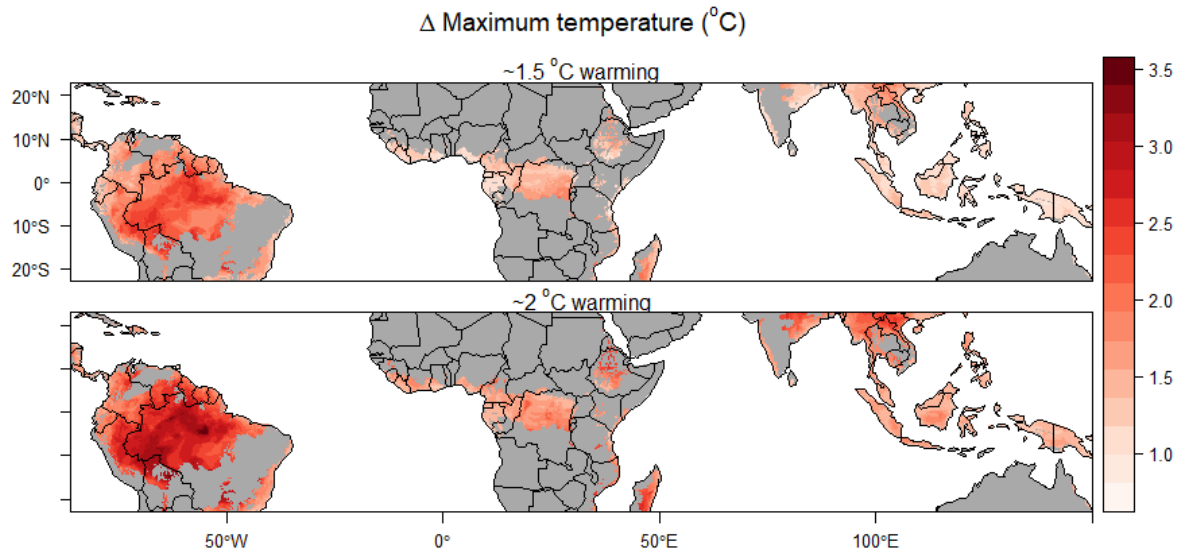
925 **Figure S11.** Variation in tropical forest aboveground carbon stocks, gains and residence time within

926 and amongst continents. Data are presented as empirical probability density functions (top row) and

927 dot-plots showing raw data points for all our multi-census plots (bottom row). SA = South America,

928 AF = Africa, AS = Asia, AU = Australia.

929



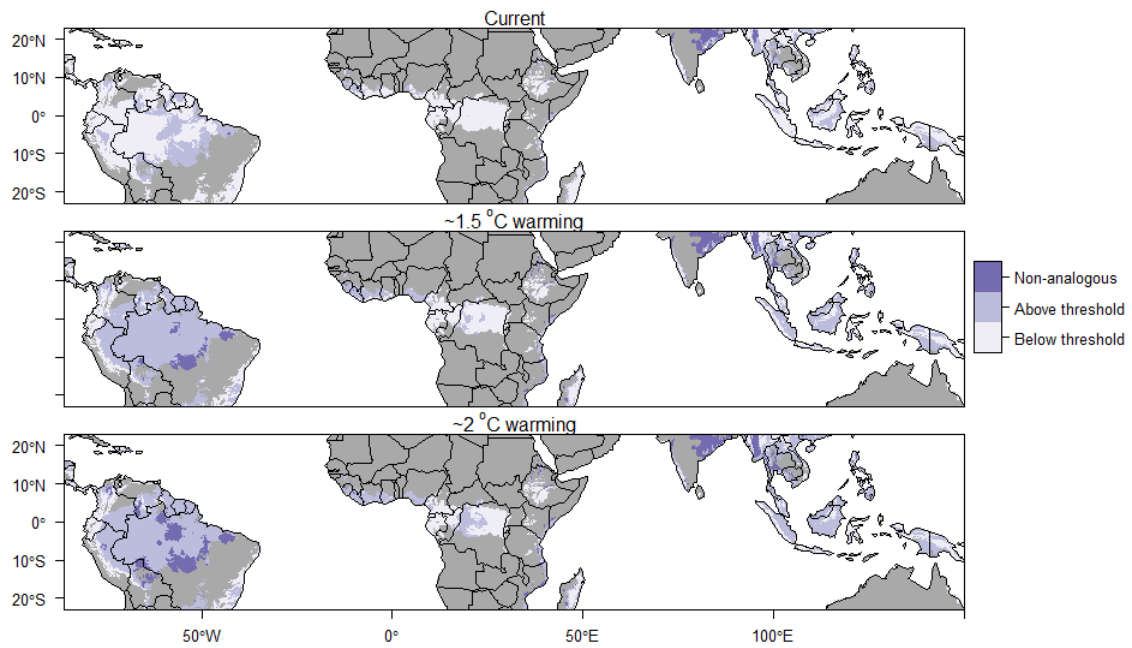
930

931 **Figure S12.** Biome-wide change in mean daily maximum temperature in the warmest month from  
932 present conditions (based on the Worldclim climatology, 1970-2000), given global increases in  
933 temperature of approximately 1.5°C and 2°C above pre-industrial levels. These levels of global  
934 temperature increase are obtained from, respectively, RCP 2.6, 2040-2060 and RCP 4.5, 2040-2060.  
935 Global temperature increases of 1.5 and 2°C above pre-industrial levels (so ~0.8 °C and ~1.3 °C  
936 above our current baseline climate) would lead to mean increases in maximum temperature in the  
937 warmest month across the tropical forest biome of 1.9°C and 2.4°C the current baseline climate  
938 respectively.

939

940

941



942

943 **Figure S13** Areas of the biome above or below the 32.2°C threshold, above which carbon stocks  
 944 decline more rapidly with temperature, under current conditions and two warming scenarios (see Fig.  
 945 4). Areas warmer than any currently observed in our dataset (35.2°C) are also shown (non-analogous  
 946 conditions). Note that even the 1.5°C warming scenario pushes most South American forests above  
 947 the 32.2°C threshold.

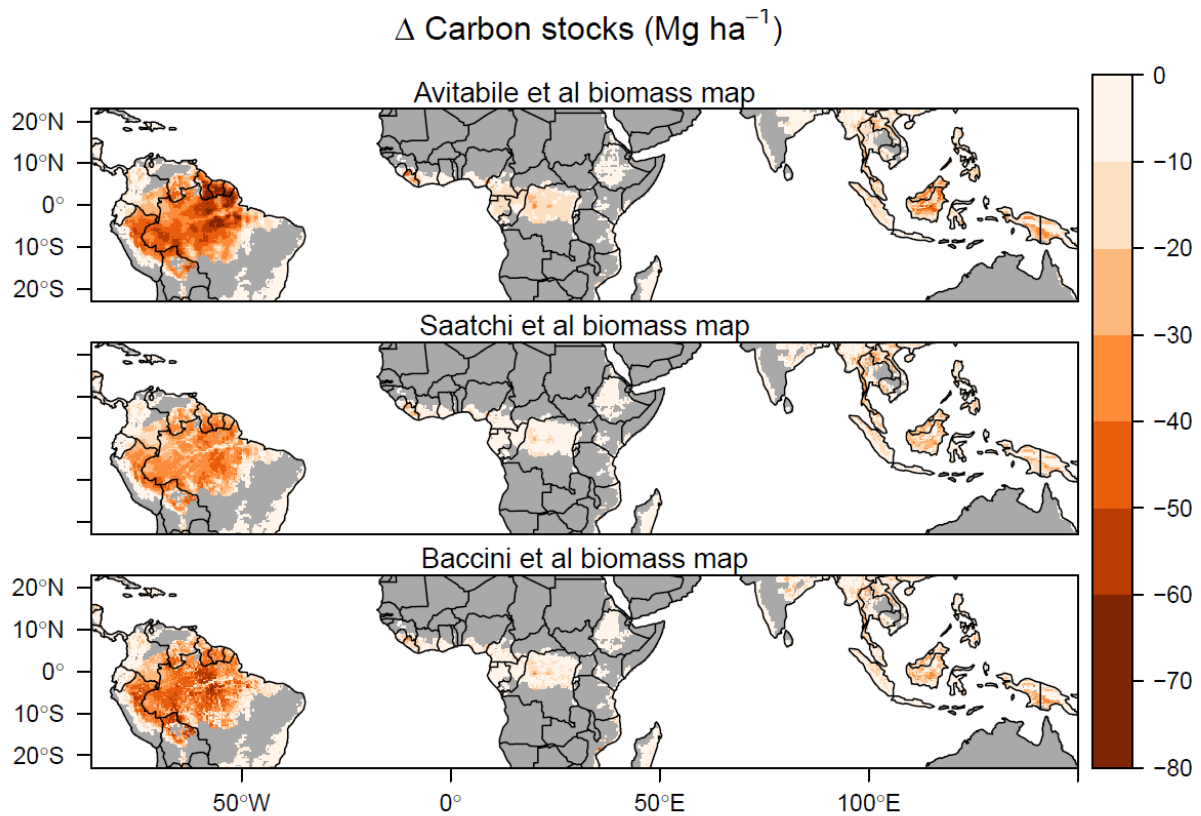
948

949

950

951

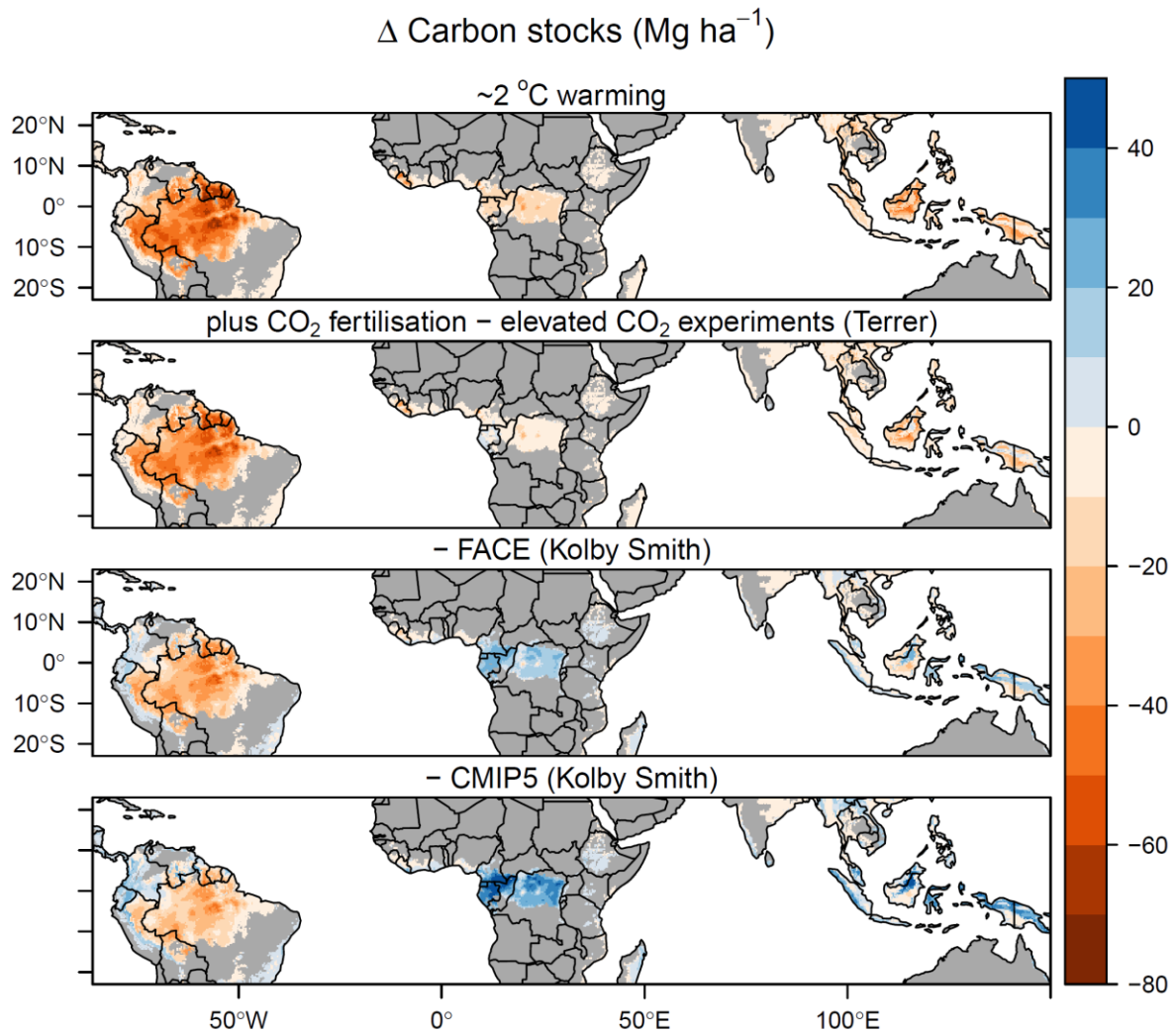
952



953

954 **Figure S14.** Effect of using earlier biomass reference maps for estimates of change in long-term  
955 carbon stocks for global temperature increases of  $\sim 2^\circ\text{C}$ . Using aboveground biomass stock maps from  
956 Saatchi et al. (65) and Baccini et al. (66) predicted biome-wide reductions in biomass carbon stocks  
957 are 24.0 Pg (95 % CI = 5.8 – 39.6) and 28.4 Pg (95 % CI = 16.1 – 37.5) respectively. Under the  $\sim$   
958  $1.5^\circ\text{C}$  warming scenario these are 18.4 Pg (5.8 – 30.5) and 21.1 Pg (10.2 – 29.4) respectively. Results  
959 in the main text use the 2016 Avitabile et al. baseline map (30) – see methods for justification.

960



961

962 **Figure S15.** Predicted long-term change in aboveground carbon stocks under ~ 2°C global warming,  
 963 based on either temperature effects alone or when also accounting for carbon dioxide growth  
 964 stimulation. CO<sub>2</sub> fertilisation effects on equilibrium biomass levels were obtained from a recent  
 965 synthesis of results of elevated CO<sub>2</sub> experiments (Terrer et al. (77)), free-air CO<sub>2</sub> enrichment (FACE)  
 966 experiments (Kolby Smith et al. (74)) and CMIP5 earth system models (Kolby Smith et al. (74)).  
 967 Depending on their strength, CO<sub>2</sub> effects either partially or fully ameliorate the biome-wide negative  
 968 effects of increasing temperatures on biomass carbon stocks (Table S3), but these carbon stocks are  
 969 predicted to decline over much of Amazonia even under the strongest CO<sub>2</sub> effect considered.

970

971

972 **Table S1.** Climate variables selected for analysis and mechanisms by which they can affect carbon stocks.

Climate property	Variable selected for analysis	Mechanism to affect carbon stocks
Daytime temperature	Maximum temperature in the warmest month <sup>1</sup>	High daytime temperatures exceed photosynthesis optima (80), increase evaporative stress, causing stomatal closure and reducing time for photosynthesis (26) and increase risk of mortality through hydraulic failure and/or carbon starvation (23).
Night-time temperature	Mean daily minimum temperature	Respiration rate increases with temperature so proportion of carbon taken through photosynthesis that is allocated to wood should decline with temperature (81). Increased respiration cost could also reduce tree longevity (23). As respiration occurs day and night, and photosynthesis only in the day, nighttime temperature should better reflect respiration effects and daytime temperature better reflect photosynthesis effects.
Moisture availability	Precipitation in the driest quarter <sup>2</sup>	Moisture availability could limit photosynthesis and hence carbon gains, with stomata closing when moisture availability is limiting. The risk of mortality through hydraulic failure or carbon starvation is higher when moisture is limiting (23), and this could also set a limit on potential tree size and hence tree longevity.
Light availability	Cloud frequency	Increased photosynthesis and hence AGWP when light availability is greatest (i.e. cloud cover is low) (82). Alternatively, light availability could have a negative effect due to high evapotranspiration stress when cloud cover is low.
Wind speed	Mean wind speed	Carbon stocks are expected to be lower where physical damage through wind throw or breakage is higher, as carbon is removed more quickly from the system through mortality (83). But there is potential for greater carbon gains if forests are more dynamic.

973 <sup>1</sup> Mean daily temperature in the warmest month (bio5) was selected instead of mean daily maximum temperature as it was more strongly decoupled from  
974 other climate variables. VPD could also represent some of these effects, but was too strongly correlation with maximum temperature to include as an  
975 independent variable.

976 <sup>2</sup> Moisture availability could also be represented by MCWD (maximum cumulative water deficit) or total precipitation, but only one of the three variables  
977 could be included in the model due to collinearity. MCWD was excluded as it is zero truncated, so less amenable to regression fitting.

978

979 **Table S2.** Coefficients of model-averaged general linear models of carbon stocks, gains and residence time as a function of climate, soil, continent and spatial  
 980 autocorrelation. Coefficients are AIC weighted averages across models with  $\Delta AIC < 4$  from the best performing model; variables are given a score of zero if  
 981 they did not appear in a model. NA indicates that a term did not occur in any model in this set. MEM1-8 are spatial eigenvectors.

Variable	Carbon stocks				Carbon gains				Carbon residence time			
	Estimate	SE	Z	P	Estimate	SE	Z	P	Estimate	SE	Z	P
Intercept - Africa	4.986	0.010	476.9	<0.001	0.571	0.525	1.09	0.278	3.909	0.688	5.67	<0.001
Minimum temperature	0.031	0.019	1.67	0.096	-0.001	0.007	0.18	0.861	0.019	0.022	0.88	0.381
Maximum temperature, warmest month	-0.089	0.022	4.11	<0.001	-0.060	0.017	3.47	<0.001	-0.001	0.015	0.10	0.924
Precipitation, driest quarter	0.045	0.018	2.54	0.011	-0.001	0.008	0.14	0.887	0.061	0.023	2.70	0.007
Cloud frequency	0.002	0.008	0.24	0.814	-0.006	0.011	0.54	0.592	0.025	0.021	1.17	0.241
Wind speed	0.004	0.012	0.38	0.705	0.016	0.020	0.78	0.437	-0.004	0.015	0.24	0.807
Soil texture (% clay)	0.021	0.017	1.26	0.208	-0.005	0.011	0.49	0.628	0.040	0.018	2.17	0.030
Soil fertility (CEC)	-0.003	0.009	0.34	0.732	0.005	0.011	0.51	0.613	-0.012	0.017	0.70	0.486
MEM1	0.115	0.014	7.96	<0.001	0.319	0.559	0.57	0.569	0.375	0.734	0.51	0.610
MEM2	0.098	0.017	5.67	<0.001	0.083	0.273	0.30	0.762	0.286	0.359	0.80	0.427
MEM3	-0.025	0.014	1.84	0.065	0.014	0.041	0.34	0.735	0.007	0.054	0.12	0.904
MEM4	-0.021	0.011	1.84	0.066	-0.038	0.020	1.84	0.066	-0.002	0.027	0.07	0.945
MEM5	0.027	0.011	2.46	0.014	0.020	0.015	1.33	0.182	0.020	0.020	0.98	0.327
MEM6	0.017	0.011	1.56	0.118	0.025	0.011	2.34	0.019	-0.014	0.014	1.05	0.293
MEM7	0.010	0.011	0.93	0.353	-0.017	0.010	1.61	0.107	0.036	0.014	2.57	0.010
MEM8	-0.072	0.013	5.64	<0.001	0.057	0.012	4.91	<0.001	-0.127	0.016	7.80	0.000
Asia	NA				0.380	0.542	0.70	0.485	-0.753	0.683	1.10	0.271
Australia	NA				-0.173	0.390	0.44	0.658	0.006	0.516	0.01	0.990
South America	NA				0.643	1.164	0.55	0.582	0.542	1.530	0.35	0.724

983 **Table S3.** Predicted biome-wide changes in long-term biomass carbon stocks (scaled to include root  
 984 biomass) under global temperature increases of ~ 1.5°C and ~ 2°C. Changes are based on temperature  
 985 effects alone, and when also accounting for the effect of increased CO<sub>2</sub> concentrations on tree growth.  
 986 CO<sub>2</sub> effects were obtained from a synthesis of results of elevated CO<sub>2</sub> experiments (Terrer et al. (77)),  
 987 free-air CO<sub>2</sub> enrichment (FACE) experiments (Kolby Smith et al. (74)) and CMIP5 earth system  
 988 models (Kolby Smith et al. (74)). 95% confidence intervals around changes (based on uncertainties in  
 989 temperature effects alone) are shown in parentheses.

CO <sub>2</sub> effect	Change in biomass carbon stocks (Pg)	
	~ 1.5°C warming (443 ppm CO <sub>2</sub> )	~ 2°C warming (487 ppm CO <sub>2</sub> )
None	-26.9 (-38.4 - -15.8)	-35.3 (-49.0 - -20.9)
Terrer et al. elevated CO <sub>2</sub> experiments	-22.0 (-33.0 - -9.9)	-26.3 (-37.6 - -11.5)
Kolby Smith et al. FACE experiments	-6.2 (-16.8 - 7.7)	-9.9 (-24.3 - 3.9)
Kolby Smith et al. CMIP5 models	3.9 (-8.3 - 12.6)	2.0 (-11.9 - 19.8)

990



Supporting information for Sullivan et al.

991

992

993